Испарение капель жидкостей и коллоидных растворов

Л.Ю. Бараш

ИТФ им. Л.Д. Ландау
МИЭМ НИУ ВШЭ

- L.Yu. Barash, Int. J. Heat and Mass Transfer, 84, 419 (2015)
- L.Yu. Barash, Int. J. Heat and Mass Transfer, 102, 445 (2016)
- L.Yu. Barash et.al., Phys. Rev. E 79, 046301 (2009)
- L.Yu. Barash, Phys. Rev. E 79, 025302(R) (2009)

5 сентября 2018 при поддержке гранта РНФ №18-71-10061 Вычислительные среды

Motivations and applications

Evaporation of liquid droplets is a quickly developing area, because it addresses both fundamental scientific problems and industrial interests.

Modern applications:

- controlling deposition of particles on solid surfaces
- micro/nano material fabrication
- manufacture of novel optical and electronic materials
- deposition of DNA/RNA micro-arrays
- biochemical assays
- disease detection via analysis of stain patterns left by drying of biological fluids
- preparing ultraclean surfaces
- ink-jet printing
- spraying of pesticides
- thin film coatings
- protein crystallography

Deposition patterns formed are influenced by a wealth of phenomena: evaporative mass transfer, heat conduction and convection, natural convection, viscous and inertial flows, surface-tension-driven flows, thermal-hydrodynamic instabilities, buoyancy effects, liquid spreading, contact-line pinning and depinning, adhesion, etc. In general, the phenomena are coupled and nonlinear, necessitating a numerical analysis to explain them.

Figure 1. A droplet placed on a solid surface. A zoom-in reveals that the contact line is pinned on the microscopically rough surface.

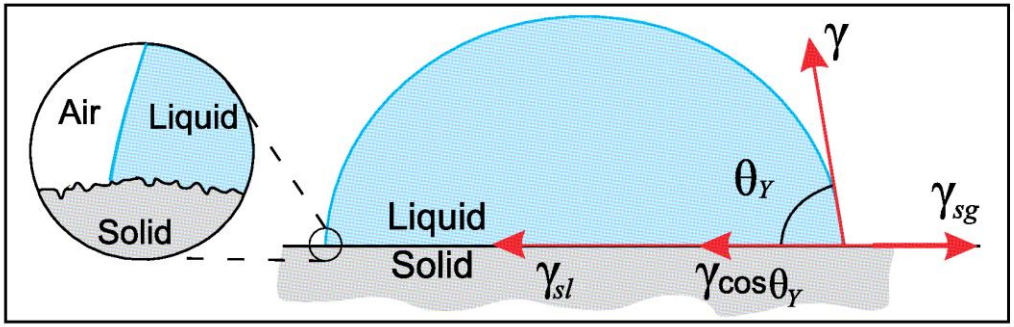

From D. Mampallil, Resonance, 19(2), 123-134 (2014)

Box 1. Surface Tension

The surface excess energy per unit area of liquid surfaces when it is in contact with another material is called surface tension or interfacial tension. When a liquid droplet is in contact with a solid (see *Figure* 1), the equilibrium forces due to the interfacial tensions at the liquid-gas (γ), the solid-gas (γ_{sg}) and the solid-liquid (γ_{sl}) interface determine the contact angle, $\theta_Y = (\gamma_{sg} - \gamma_{sl})/\gamma$ of the droplet on the solid. Droplets placed on solid surfaces, therefore, adopt spherical to flat shapes depending upon the interfacial tensions. The lower the surface tension γ, the higher the tendency of a liquid to spread on a given solid surface. Another consequence of the surface tension is the excess pressure (compared to the outside pressure) inside a droplet or a bubble (see also *Figure* A). This is called Laplace pressure given by $\triangle P = P_{\text{inside}} - P_{\text{outside}} = 2\gamma/R$, for a spherical droplet of radius R. The smaller the droplet, the greater its inner pressure. For a water droplet of 1 μ m radius, $\triangle P$ can be as high as atmospheric pressure*.

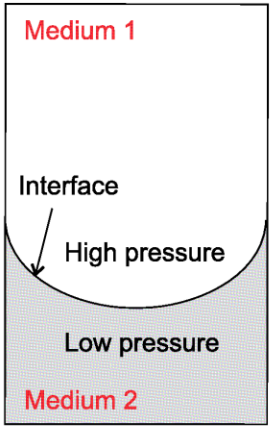

Figure A. Pressure varies across a curved interface separating two fluid mediums. The low- and high- pressure regions are shown (relative to each other).

* Pierre-Gilles de Gennes, Françoise Brochard-Wyart and David Quéré, *Capillarity and wetting phenomena: drops, bubbles, pearls, waves*, Springer, Chapter 1, 2004.

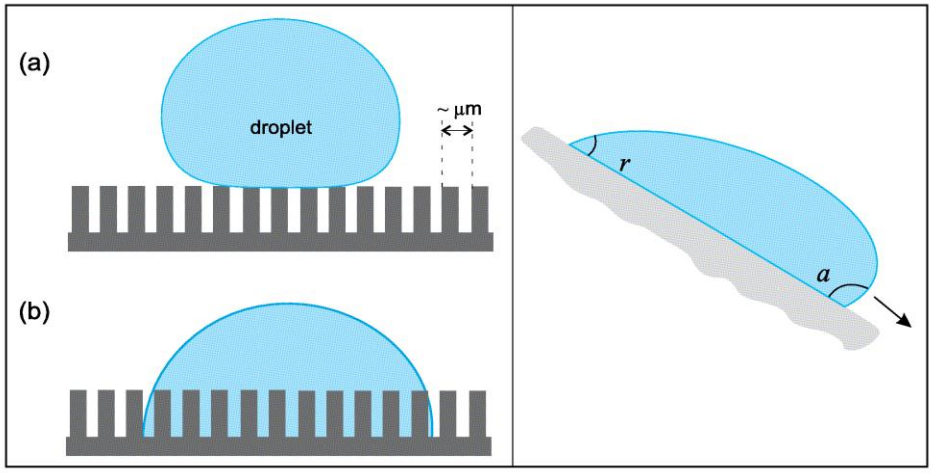

Figure 2 (left). Structure of a super-hydrophobic surface where a droplet sits partially in the air (Cassie Baxter state). Under certain conditions (see text) the droplet fills in between the pillars (Wenzel state).

Figure 3 (right). A droplet flowing down on a tilted surface by gravity. The advancing and the receding contact angles are shown.

From D. Mampallil, Resonance, 19(2), 123-134 (2014)

Box 2. Super-Hydrophobic Surfaces

Super-hydrophobic surfaces are hydrophobic surfaces with some textures on them. Due to these textures, droplets sit partially on air as illustrated in *Figure* 2. Such surfaces consist of an array of pillars having a few micrometers height and separation between them. Once this array of pillars is coated with a thin film of hydrophobic material (often Teflon), a super-hydrophobic surface is obtained.

In laboratories such surfaces are made using nano-fabrication techniques. You can make super-hydrophobic surfaces at home! Take a metal spoon (or any other surface that does not burn) and hold it above a candle flame for a few seconds to form a black layer of carbon soot on the inside surface of it. Place a very small water droplet on this black layer. You can see that the droplet is spherical and rolls over the surface when you move the spoon. Here, the tiny carbon particles act as the pillars*.

* Xu Deng, Lena Mammen, Hans-Jürgen Butt and Doris Vollmer, Candle Soot as a Template for a Transparent Robust Superamphiphobic Coating, *Science*, Vol.335, pp.67–70, 2012.

Figure 4. Schematic (not to scale) of the contact angle and the radius of an evaporating droplet with time. The solid curve represents a sliding contact line and the dashed curve represents a pinned contact line during the evaporation. The evaporation time t_0 is shown. When the contact line is pinned (e.g., on a hydrophilic surface) the evaporation is quicker. The dashed vertical lines separate different phases of the evaporation.

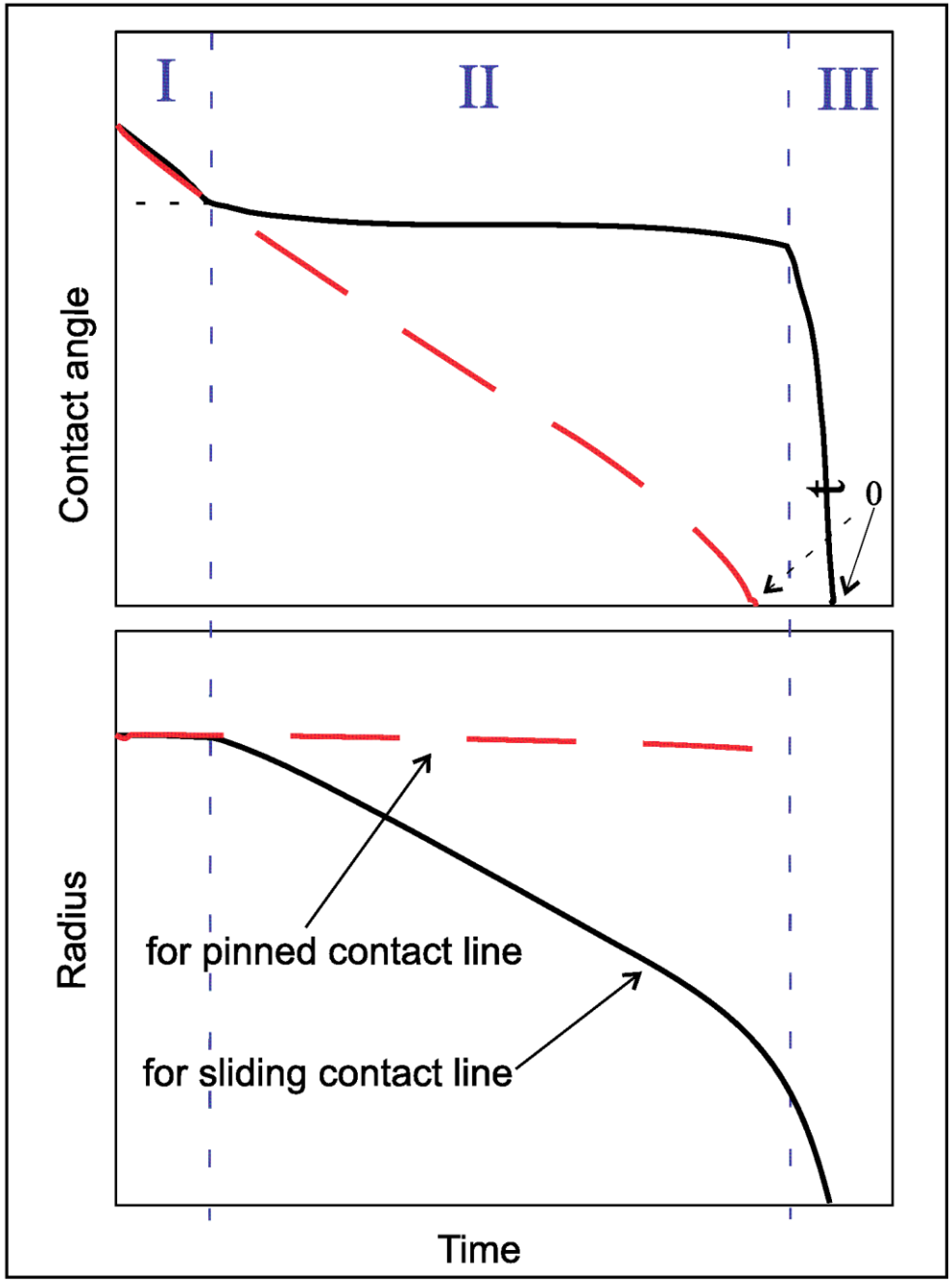

From D. Mampallil, Resonance, 19(2), 123-134 (2014)

Figure 5. An evaporating droplet with the contact line pinned on the surface. The arrows above the droplet represent the evaporation flux which diverges at the contact line. The radius of the droplet is constant while the height *h* decreases with time. The flow of liquid to compensate for the evaporated liquid from the edge is represented with the arrows inside the droplet. This flow brings the dispersed particles to the edge forming the 'coffee ring' at the end of the evaporation.

From D. Mampallil, Resonance, 19(2), 123-134 (2014)

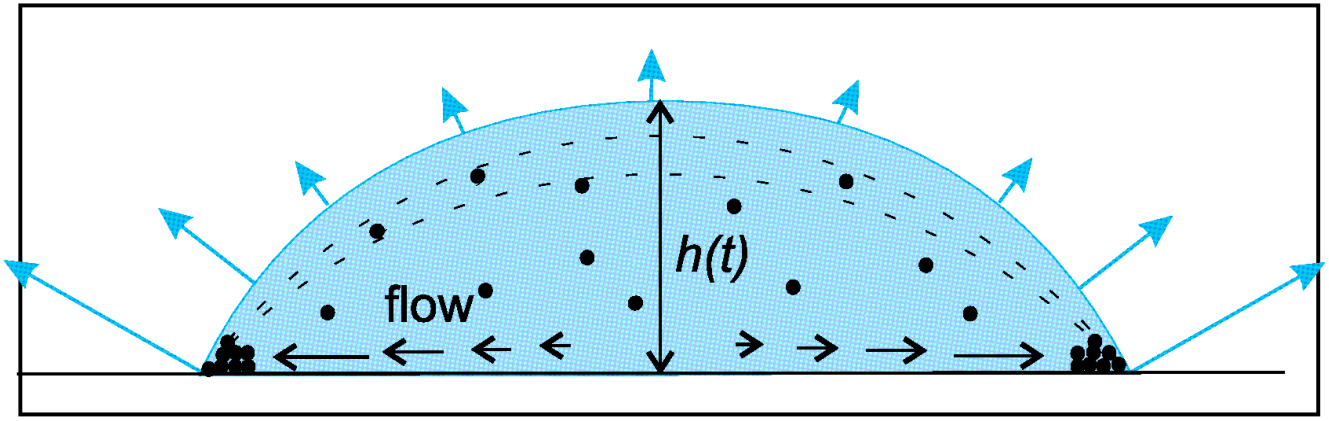

Figure 6. The capillary attractive force between two particles is illustrated. The liquid evaporation between the particles causes the meniscus to be curved more, thereby creating a low pressure region there. Consequently, the liquid flowing in from the sides brings the meniscus back to the normal shape (dash line). This flow pushes the particles towards each other.

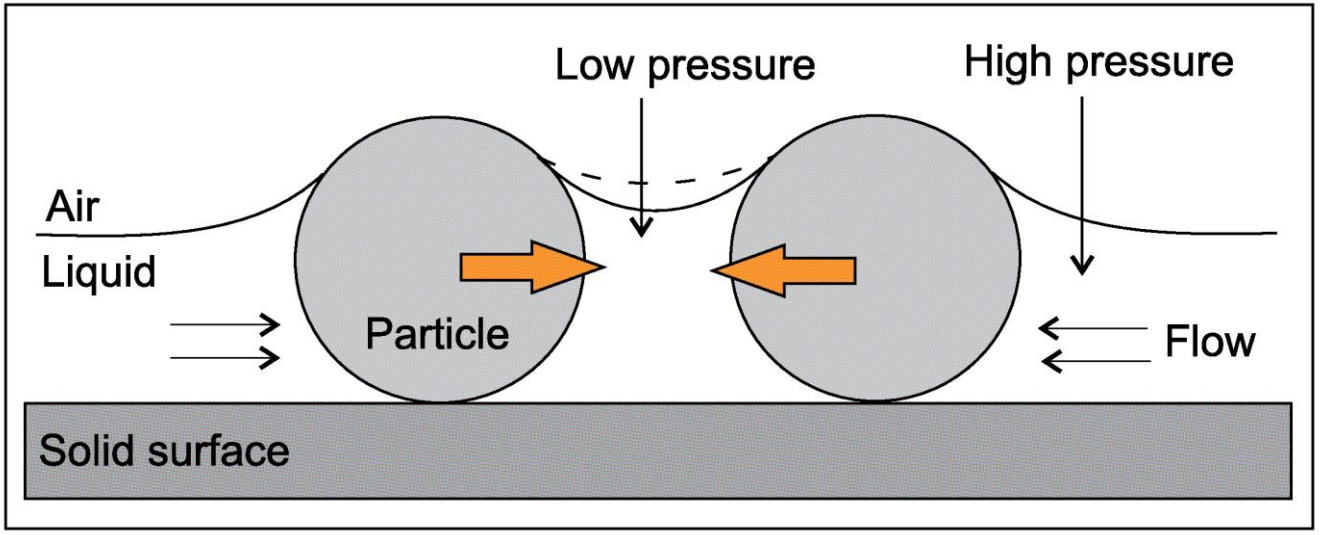

- Конвекция Марангони: гексагональная ячеечная конвективная структура в плоских жидких пленках

$$M_a = \frac{-\frac{\partial \sigma}{\partial T}(c_V \Delta T)h}{\nu k} \qquad \lambda = \frac{2\pi h}{\sqrt{M_a/8}}$$

Pearson, J. Fluid Mech., 4 (1958) 489

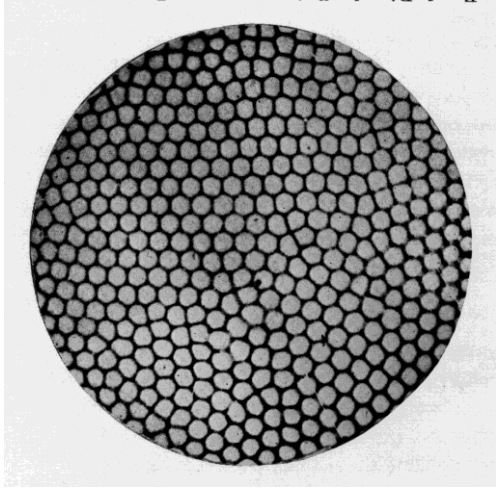

Поверхностное натяжение и температура

$$\sigma(T) = \sigma_0 - \sigma'(T - T_0)$$

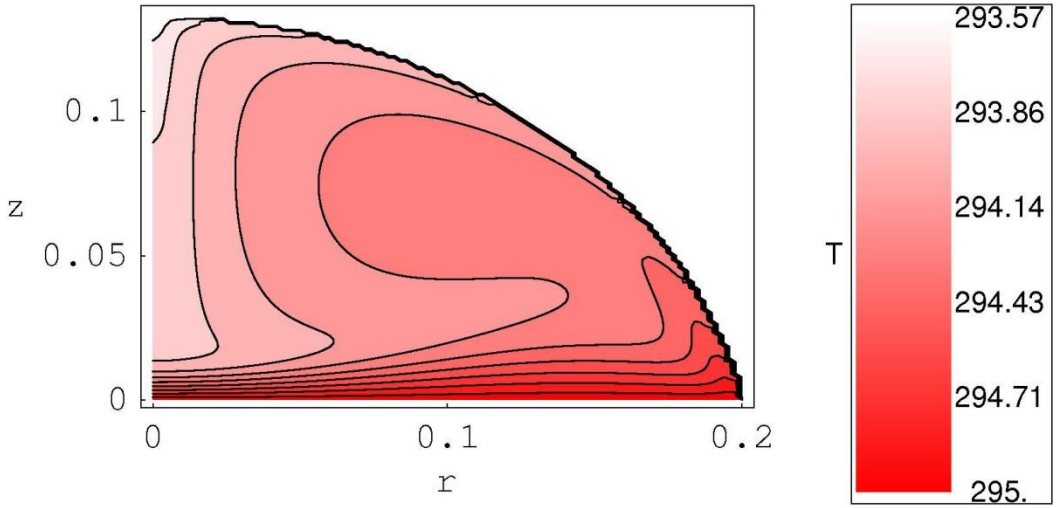

Methods for suppressing the coffee ring effect

to obtain a uniform deposition pattern

- adding chemical components
- choosing substrate with low thermal conductivity
- adding surfactants
- employing ellipsoidal particles
- employing super-hydrophobic surface (results in depinning of the contact line)
- employing electrowetting with alternating current
- adding air bubbles into the droplet
- employing MHz surface acoustic waves in the substrate (acousto-wetting)
- changing the charge of particles (results in an electrostatic attraction of partcles into the surface)
- drying a water droplet in an ethanol wapor

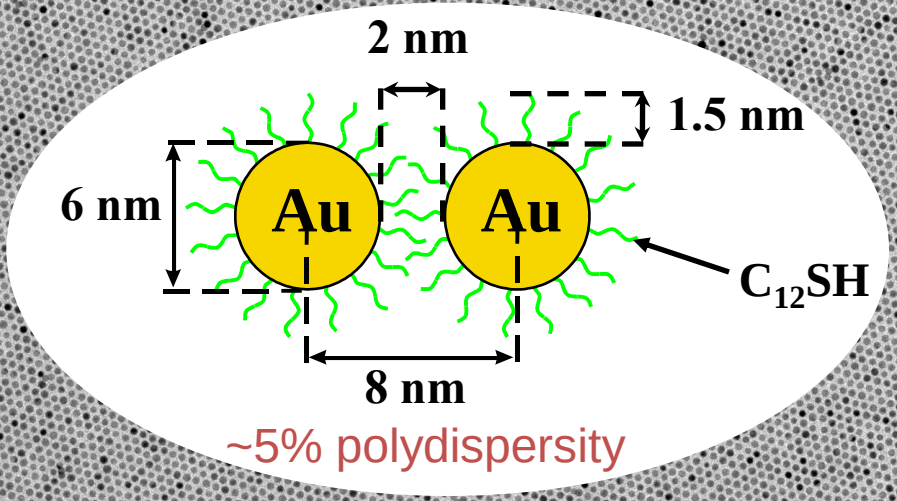

~5% polydispersity

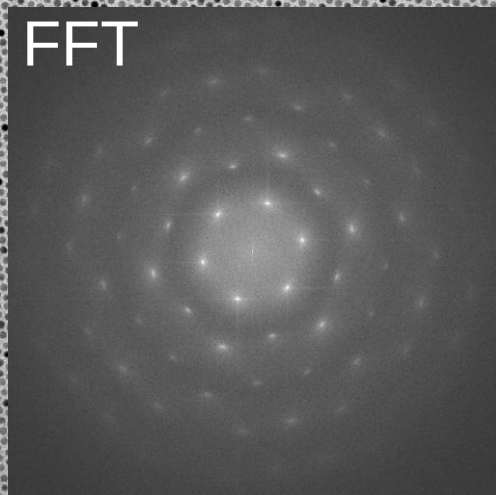

200 nm

Theory: Dimensionless Numbers

$$Ca = \frac{\eta \overline{u}}{\sigma} \ll 1$$

$$Bo = \frac{\rho g h_0 R}{2\sigma \sin\theta} \ll 1$$

$$St^{-1} = \frac{\rho C_p \overline{u} R}{k} \ll 1$$

$$\frac{B}{Ma} = \frac{\rho g h^2 \beta}{7(d\sigma/dT)} \ll 1$$

$$t_{heat} = Rh_0/\kappa \ll t_f$$

$$t_{mom} = \rho R h_0/\eta \ll t_f$$

$$t_{mass} = (\rho_{vap}/\rho_f) t_f \ll t_f$$

For small (not larger than several mm-radius) droplets of moderately volatile liquids (e.g., drying times of minutes to hours) drying in stagnant air with pinned contact line:

The droplet surface is a spherical cap.

Heat convection is slow compared to heat diffusion.

Bouyancy-driven convection is much weaker than Marangoni flow.

Heat, mass, and momentum transfer are quasi-steady state processes.

We consider laminar flow. We do not assume that the flow is a Stokes flow. $Re = \rho \overline{u} R/\eta$ is not assumed to be much smaller than unity.

Задача о форме капли при учете силы тяжести и гидродинамических эффектов

Роль отклонений от формы сферической чаши

$$B_o = \frac{\rho g h r_0}{2\sigma \sin\theta} \sim 1$$

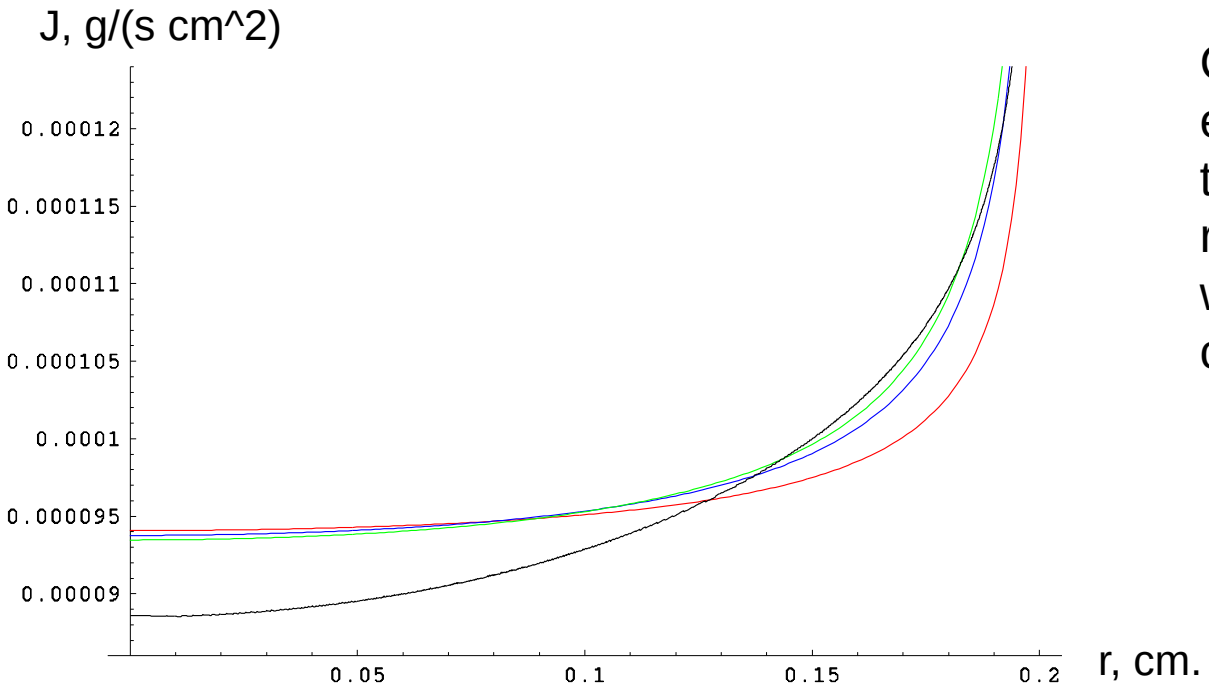

Contrary to the total evaporation rate, the local evaporation rate is not described well with the spherical cap approximation.

The curvature of the sessile drop varies along the surface in about 1.5 times

Форма лежащей капли

The Laplace equation:

$$k\sigma + \rho g z = const$$

$$k + \frac{2f}{a^2} = const$$

Capillary constant for toluene:

$$a = \sqrt{\frac{2\sigma}{\rho g}} \approx 0.26 \text{ cm}$$

For drop with rotational symmetry, we have: $z = f(x,y) \Rightarrow z = f(r)$

$$k = -\mathrm{Tr}(G^{-1}Q) = \quad (1)$$

$$= \frac{2f_x f_y f_{xy} - f_{xx}(1+f_y^2) - f_{yy}(1+f_x^2)}{(1+f_x^2+f_y^2)^{3/2}} = \quad (2)$$

$$= \frac{f''}{(1+f'^2)^{3/2}} + \frac{f'}{r(1+f'^2)^{1/2}} \quad (3)$$

G,F – matrixes of first and second quadratic forms of the surface.

$$R_2 = r / \sin\varphi$$

$$\sigma\left(\frac{1}{R_1} + \frac{\sin\varphi}{r}\right) = \frac{2\sigma}{R_0} - \rho g z$$

Unknowns: $r = r(s), \qquad z = z(s)$

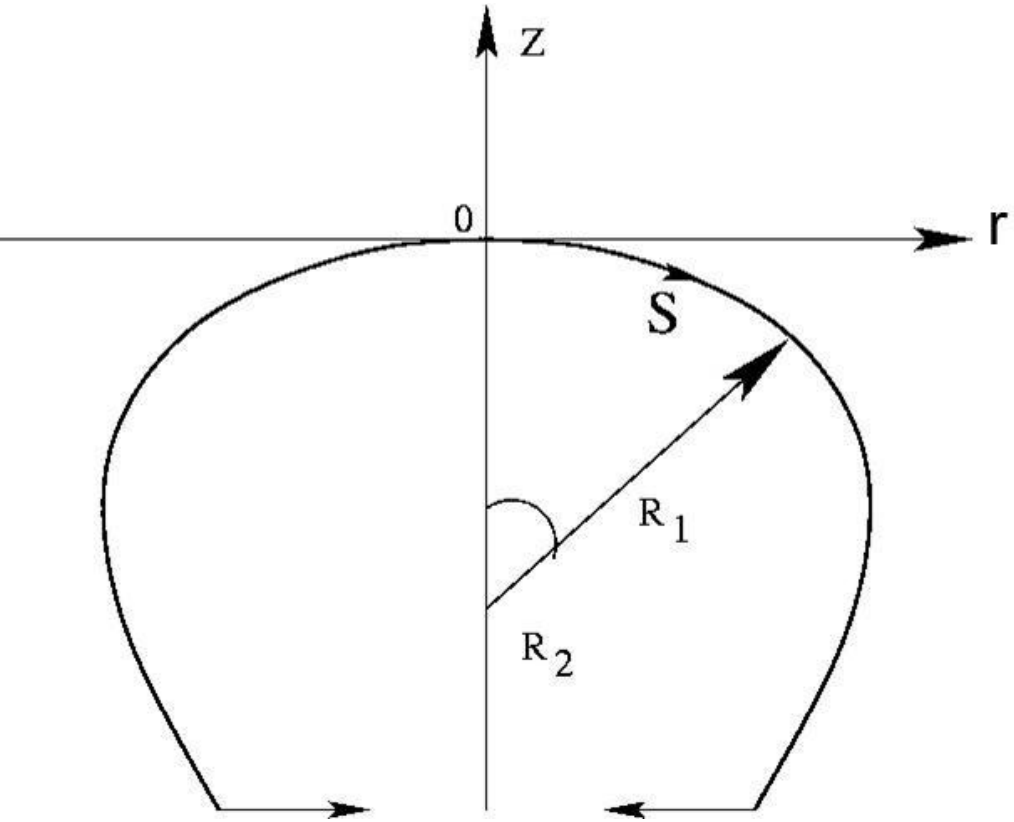

$$\dot{\varphi} = \frac{2}{R_0} - \frac{2z}{a^2} - \frac{\sin\varphi}{r}$$

$$\ddot{x} = \dot{z}\left(\frac{2}{R_0} - \frac{2z}{a^2} + \frac{\dot{z}}{r}\right)$$

$$\ddot{z} = -\dot{x}\left(\frac{2}{R_0} - \frac{2z}{a^2} + \frac{\dot{z}}{r}\right)$$

$$z(0) = 0, \quad \dot{z}(0) = 0,$$

$$r(0) = 0, \quad \dot{r}(0) = 1,$$

$$(\dot{z}/r)_{s=0} = -1/R_0.$$

Диффузионная модель испарения капли.

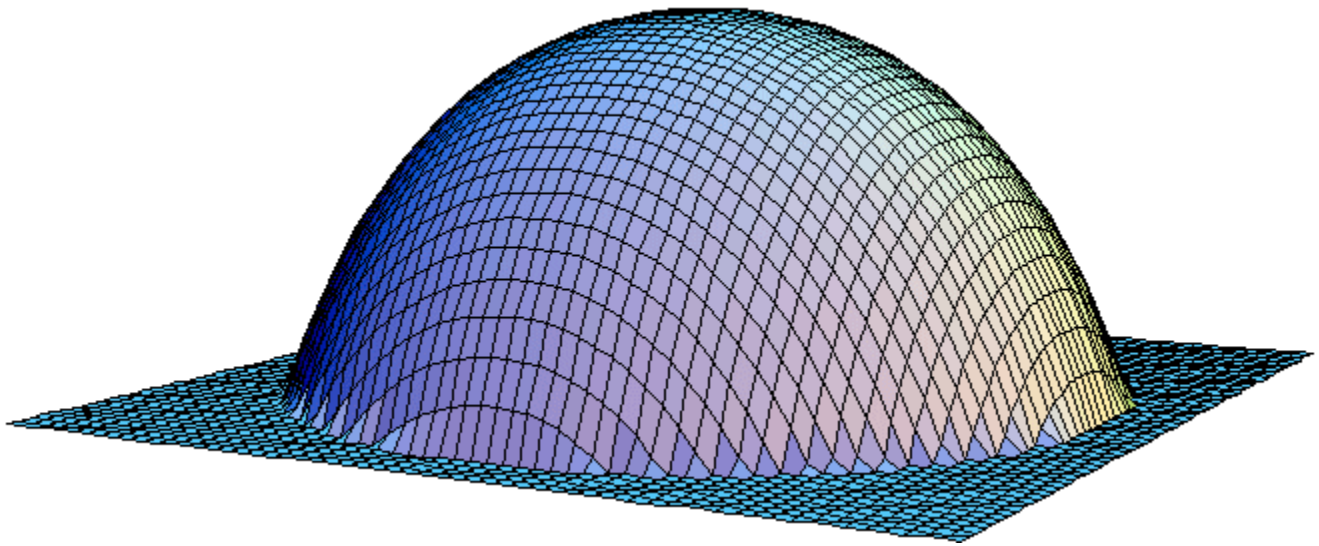

Моделирование испарения капли

$$\frac{\partial u}{\partial t} = D\Delta u$$

Часто используют приближение $\Delta u = 0,$ мотивируя тем, что $t = R^2/D \ll t_{evap}.$ На самом деле релаксация к равновесию происходит очень медленно $(\propto 1/\sqrt{t}),$ отклонения от стационарности оказываются заметны и даже в конце процесса испарения превышают 1%.

$$J = |D\nabla u|$$

Аналитическое решение

Используя приближение $\Delta u = 0$, а также приближение поверхности капли, близкой к поверхности сферы, пользуясь формулами
Deegan et. al. (Phys.Rev.E 62 (2000), 756)
Lebedev N.N. (Special Functions and their applications, NJ, 1965)
можно найти

$$u(\alpha,\beta) = u_\infty + (u_s - u_\infty)\sqrt{2(\mathrm{ch}\alpha - \cos\beta)}\int_0^\infty \frac{\mathrm{ch}\theta\tau}{\mathrm{ch}\pi\tau}\frac{\mathrm{ch}\beta\tau}{\mathrm{ch}(\pi-\theta)\tau}P_{-1/2+i\tau}(\mathrm{ch}\alpha)d\tau.$$

$$r = \frac{R\sinh\alpha}{\cosh\alpha - \cos\beta}, \qquad z = \frac{R\sin\beta}{\cosh\alpha - \cos\beta}.$$

$$J(\xi,\theta) = |D\nabla u| = \frac{Du_s}{R}\left(\frac{\sin\theta}{2} + \sqrt{2}(x(\xi,\theta)+\cos\theta)^{3/2}\times\right.$$
$$\left.\times\int_0^\infty \frac{\cosh\theta\tau}{\cosh\pi\tau}\tau\tanh(\pi-\theta)\tau P_{-1/2+i\tau}(x(\xi,\theta))d\tau\right).$$

$$m = \frac{\rho\pi R^3}{6}\tan\frac{\theta}{2}\left(3+\tan^2\frac{\theta}{2}\right), \qquad \left|\frac{dm}{dt}\right| = 2\pi R^2\int_0^1 \frac{\xi J(\xi,\theta)d\xi}{\sqrt{1-\xi^2\sin^2\theta}}.$$

$$J_s(r) = \frac{Du_s}{R}\left(\frac{\sin\theta}{2} + \sqrt{2}(x(r)+\cos\theta)^{3/2}\times\right.$$

$$\left.\times\int_0^\infty \frac{\cosh(\theta\tau)}{\cosh(\pi\tau)}\tau\tanh((\pi-\theta)\tau)P_{-1/2+i\tau}(x(r))d\tau\right), \quad (1)$$

where $x(r) = \left(r^2\cos\theta/R^2 + \sqrt{1-r^2\sin^2\theta/R^2}\right)/(1-r^2/R^2)$ and $P_{-1/2+i\tau}(x)$ is the Legendre polynomial.

It was shown in Deegan et. al. PRE 62, 756 (2000) that (1) can be approximated with high accuracy as

$$J_s(r) = J_0(\theta)(1-r^2/R^2)^{-\lambda(\theta)}, \text{ where } \lambda(\theta) = 1/2-\theta/\pi. \quad (2)$$

refined in Chini, Amirfazli, Adv. Colloid Int. Sci. 243, 121 (2017), and in Carrier et.al., J. Fluid Mech., 798, 774 (2016).

$$J(r,t) = J(r,\infty)\left(1 + \frac{Ar_0}{2\sqrt{Dt}}\right)$$

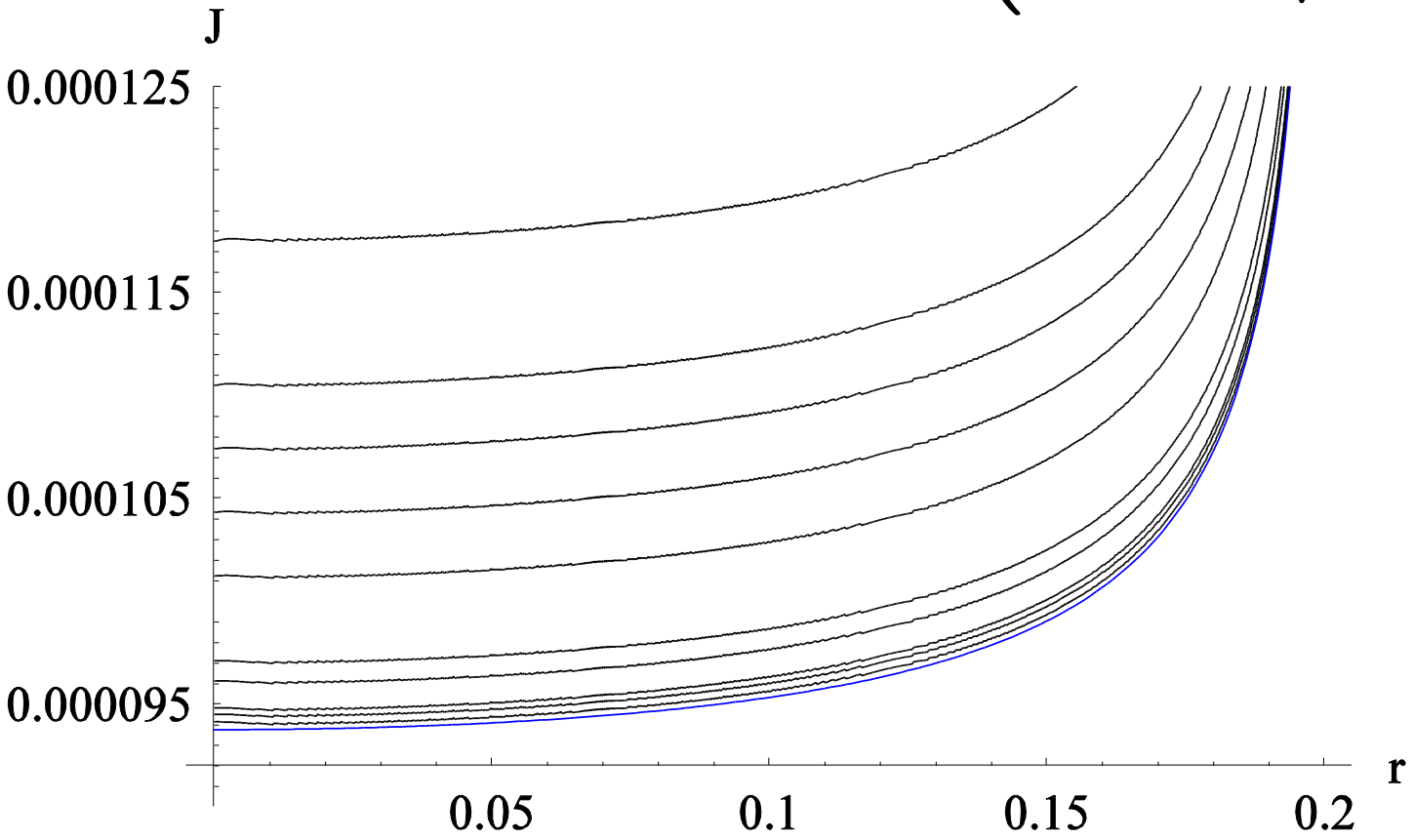

t=1,2,3,5,10,50,100,500,1000,4000 sec.

Нестационарное испарение для фиксированной поверхности в виде лежащей капли и сферической чаши

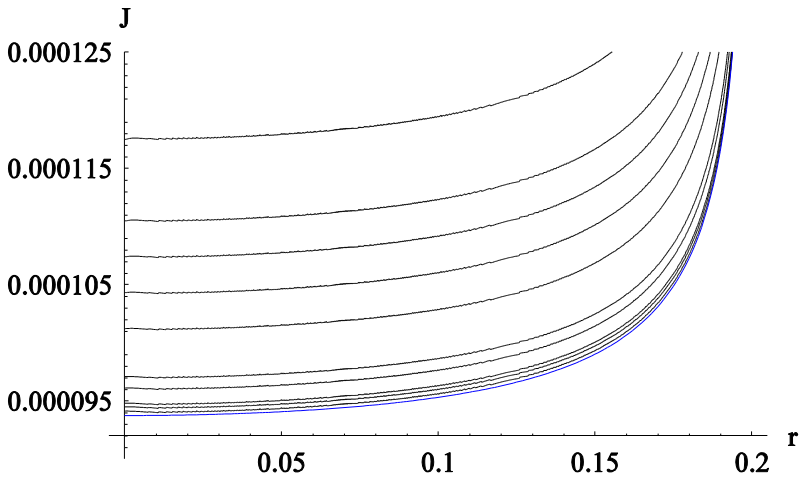

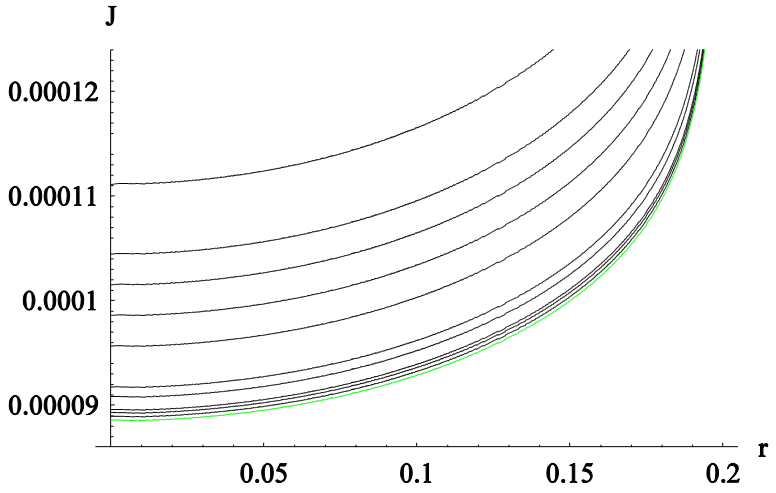

Comparing with experiment

(from L.Yu.B. et.al., PRE 79, 046301 (2009)).

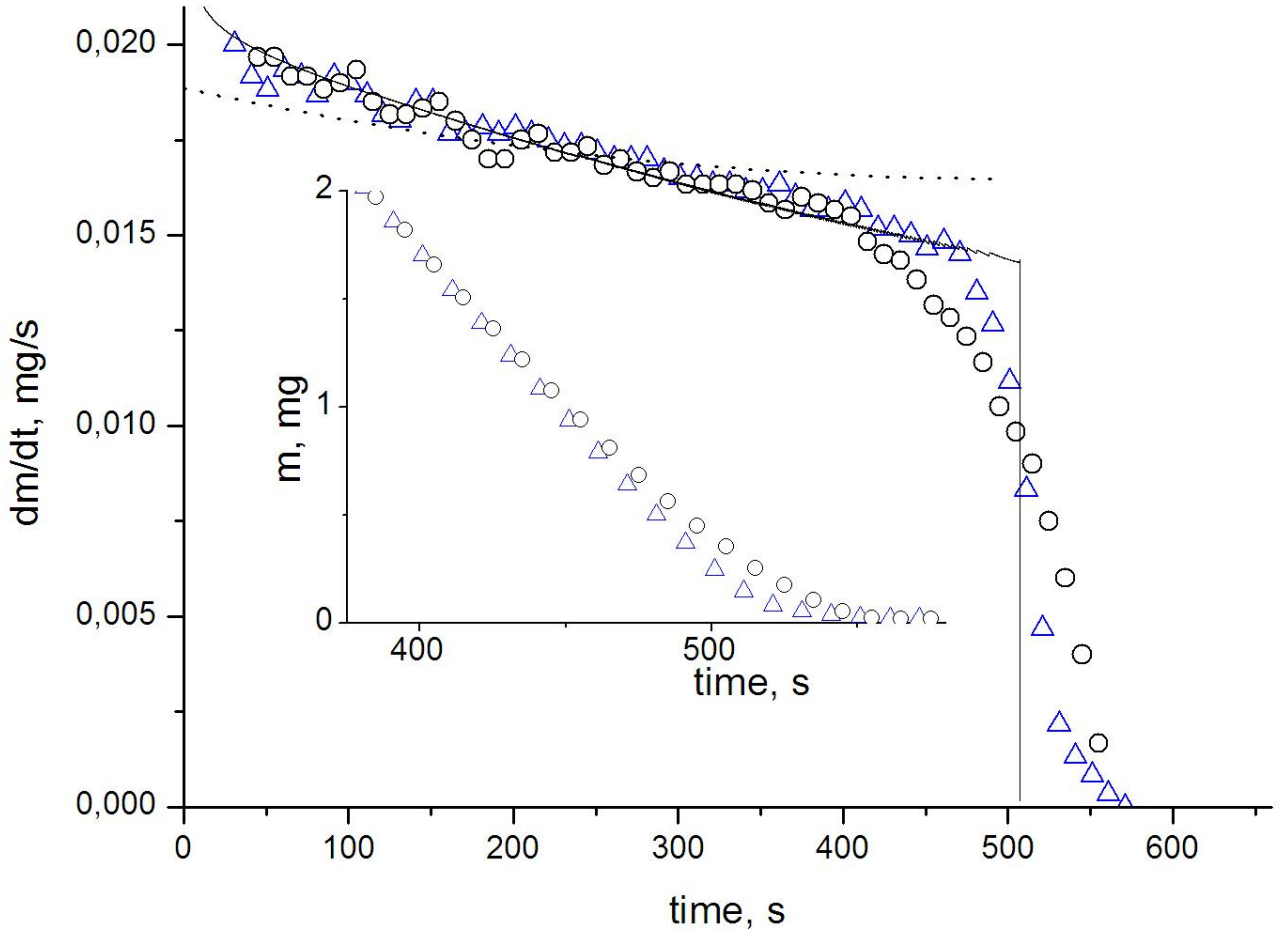

Drop evaporation rate dm/dt. Experimental data for the pure toluene evaporation (open circles) and Au nanoparticle colloid (open triangles). The solid line describes simulation results obtained within the full numerical scheme for the vapor diffusion. The dotted line is obtained assuming the local evaporation flux to be uniform over the drop surface and constant with time. Inset: Mass variation at the end of evaporation.

Xiao-Min Lin et al. использовали рассеяние пучка рентгеновских частиц на малые углы, чтобы показать, что нанокристаллы образуются на верхней поверхности капли

Narayanan, Wang, Lin, *PRL* **93**, 135503 (2004).

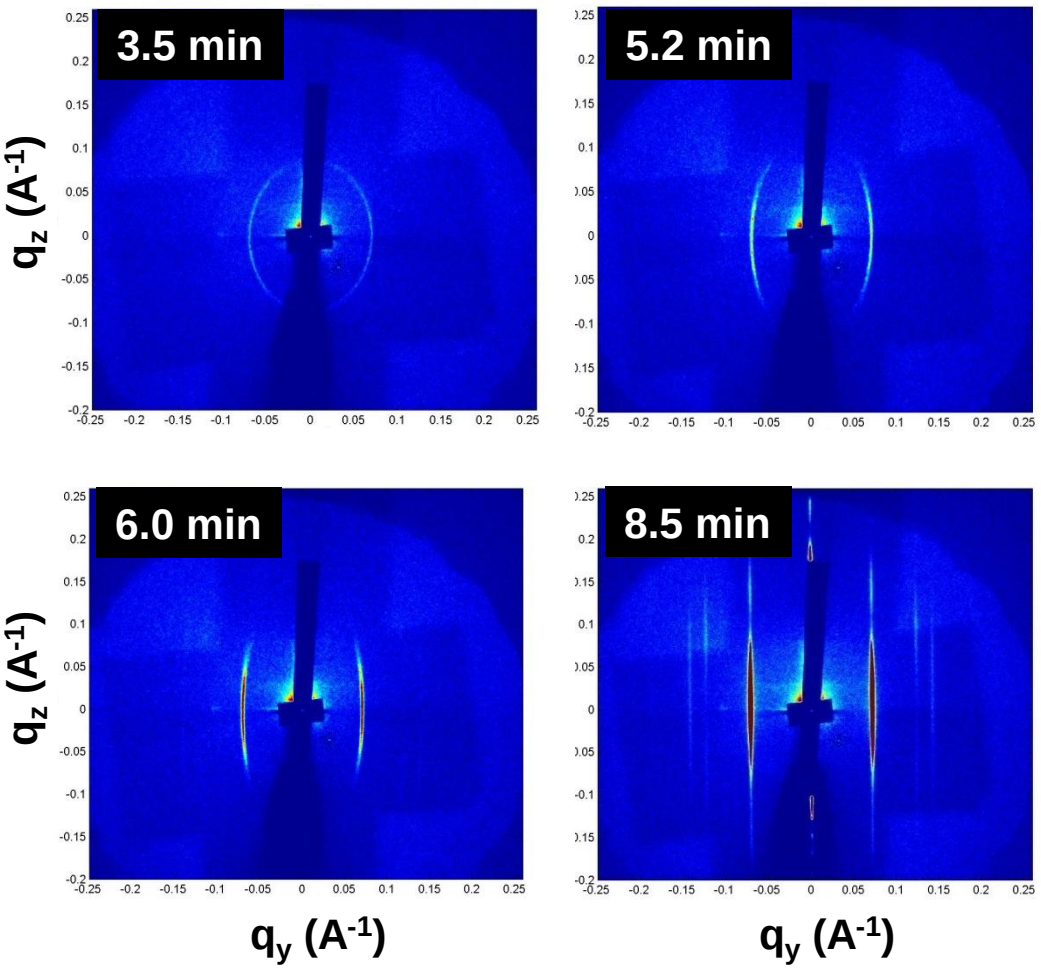

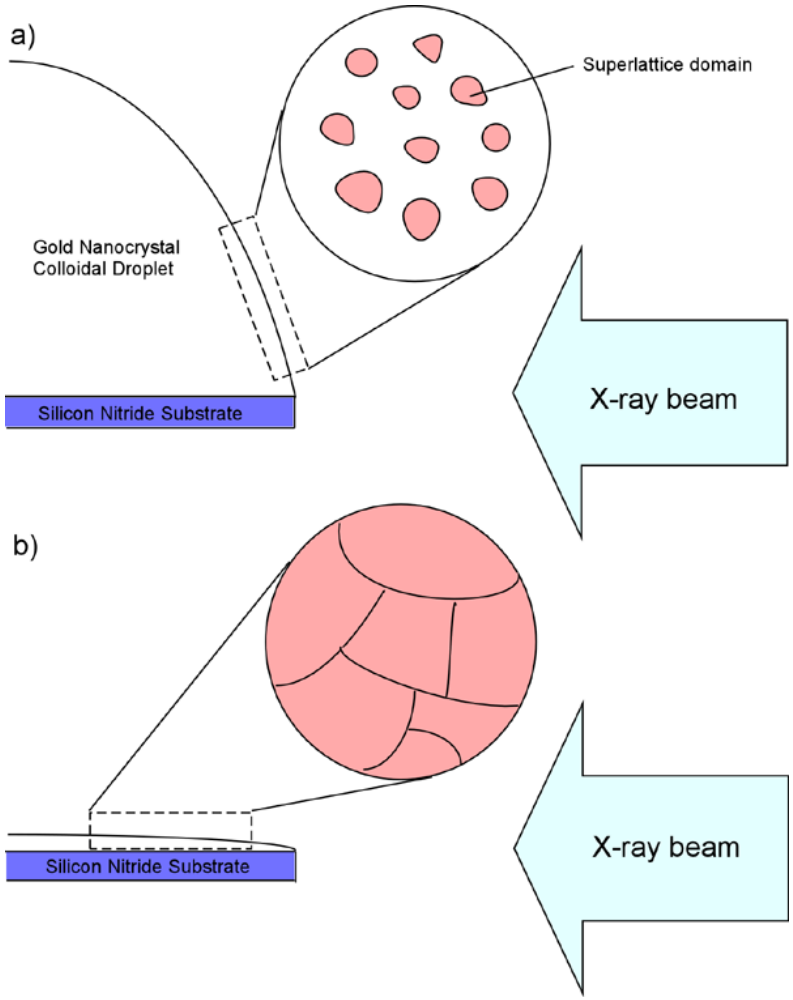

Контактные углы

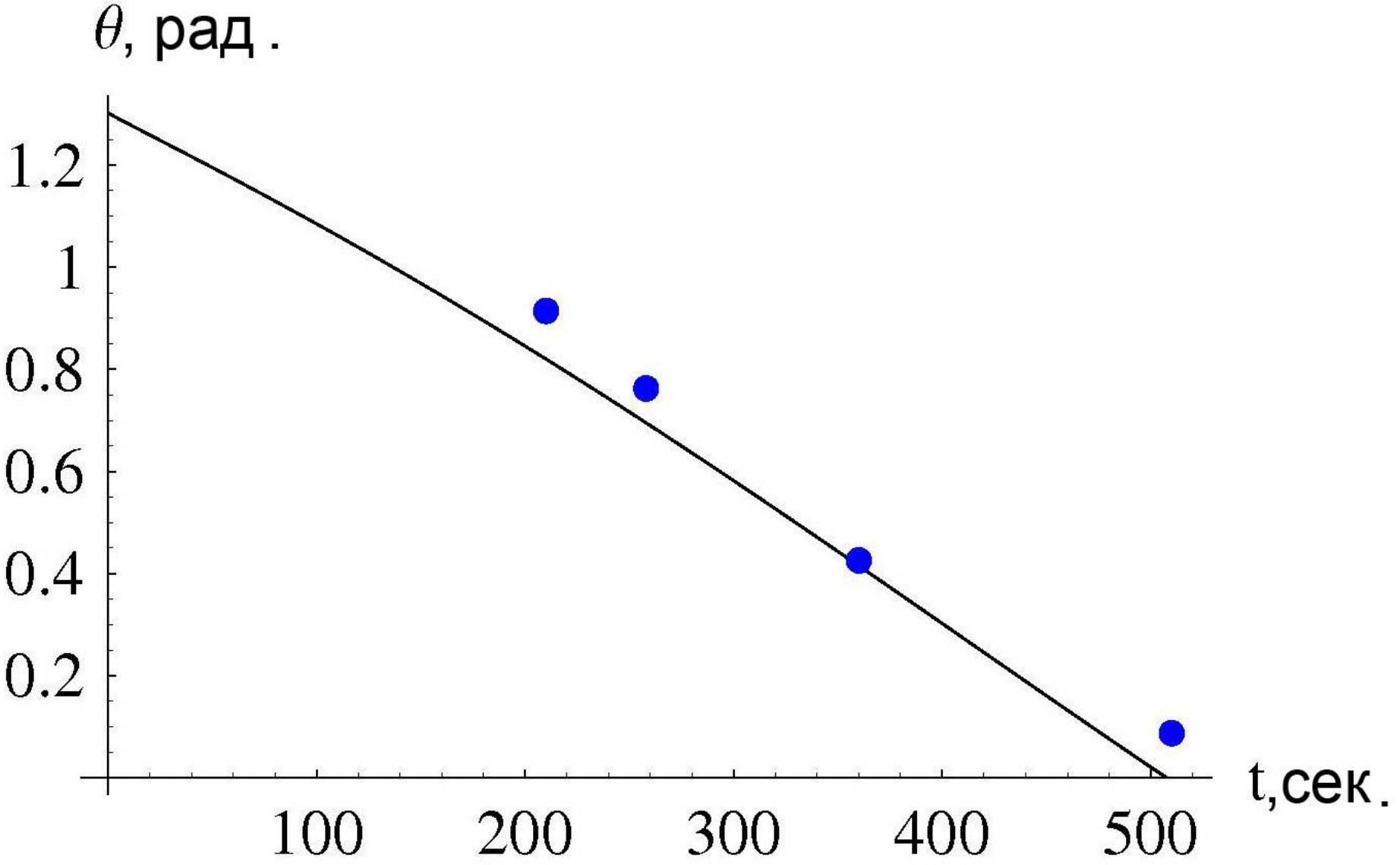

Конвекция Марангони и вихревые структуры в испаряющейся капле

Применение критерия Марангони для капли

$$M_a \approx 2800 \qquad R_e \approx 62$$

Турбулентности нет, экспериментально (для капель воды)
Турбулентность возникает при Ma>22000

$$\lambda \sim 0.03cm$$

Конкуренция конвекций за счет плавучести и сил Марангони:

$$B = \rho g h^2 \beta / (7.14\ \partial\sigma/\partial T) \approx 0.02 \ll 1$$ [Pearson,1958]

β - коэффициент теплового расширения,

Приповерхностные вихри. Поле скоростей для t=0.16 s

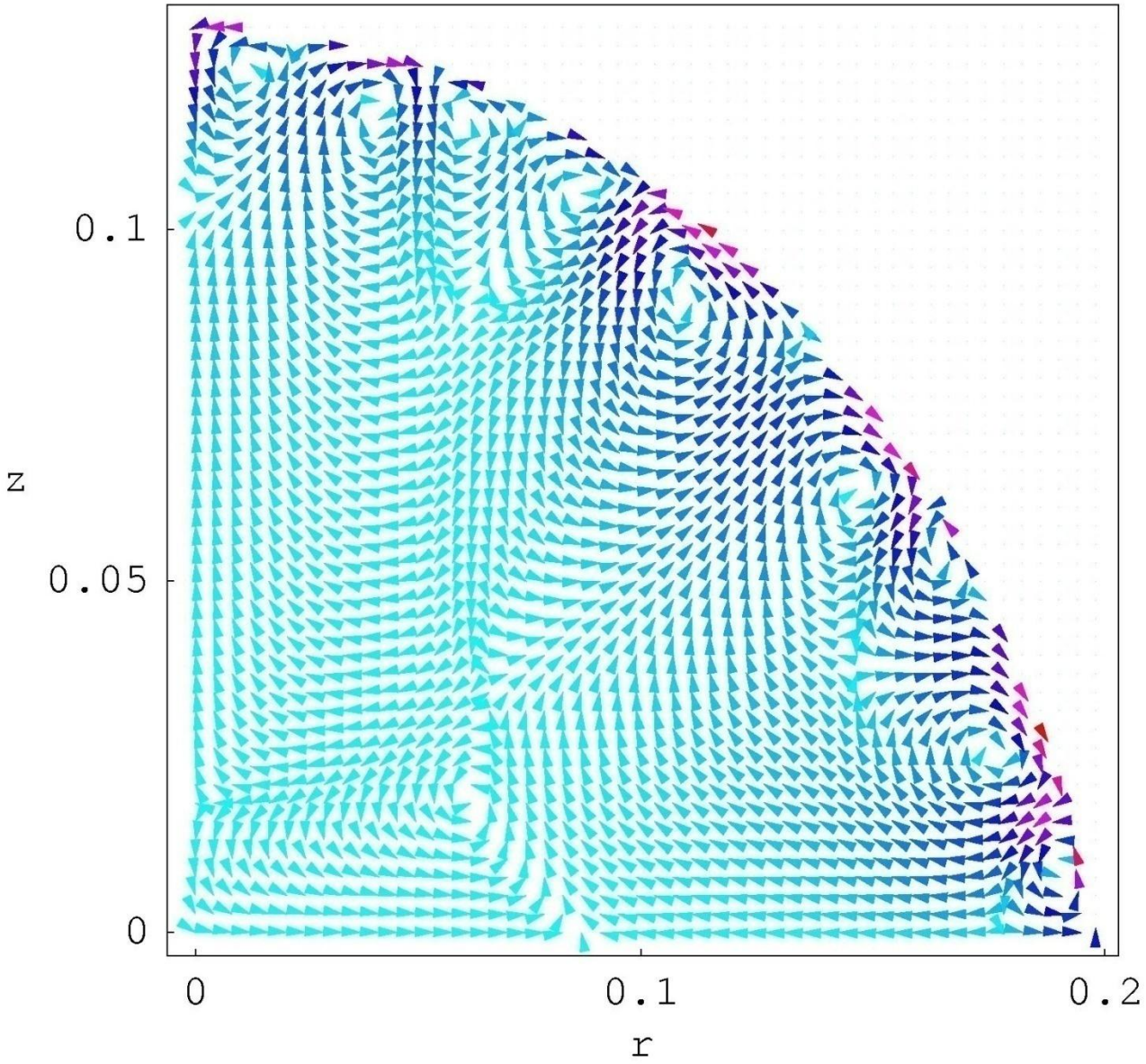

Приповерхностые вихри и распределение температуры вдоль поверхности.

z

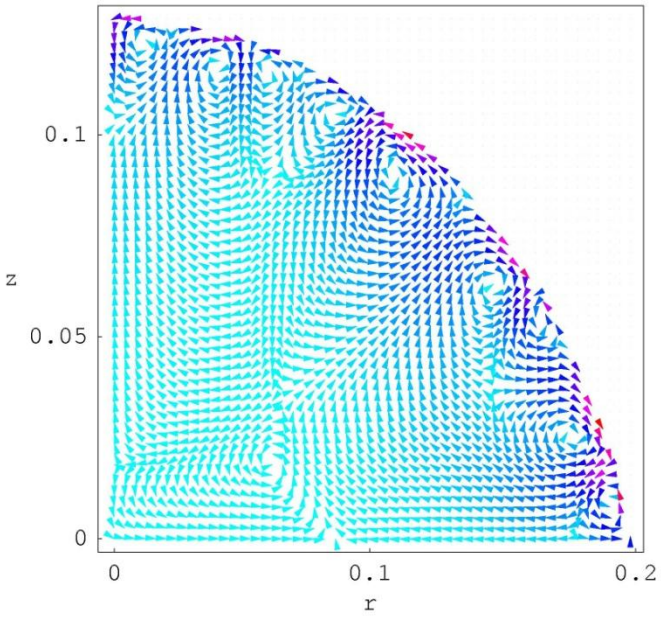

скорости

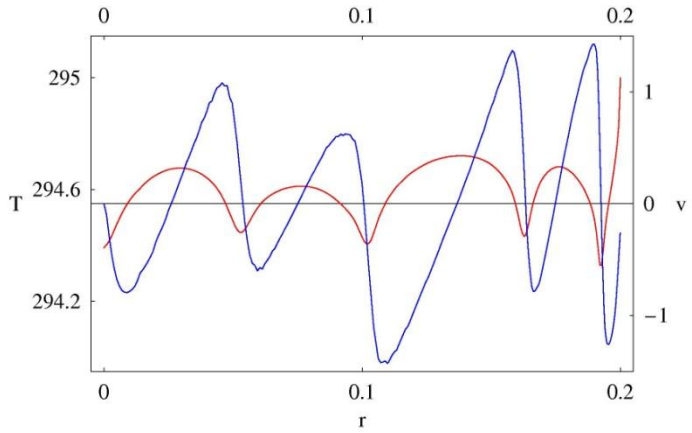

температура вдоль поверхности и скорости

r

Скорости и температура в режиме трех и одного вихрей

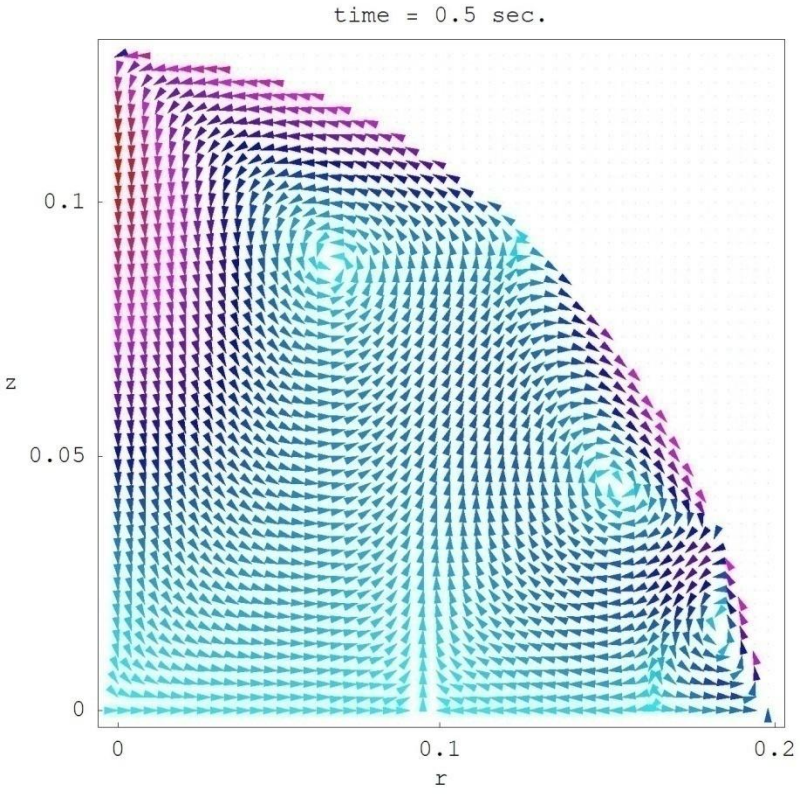

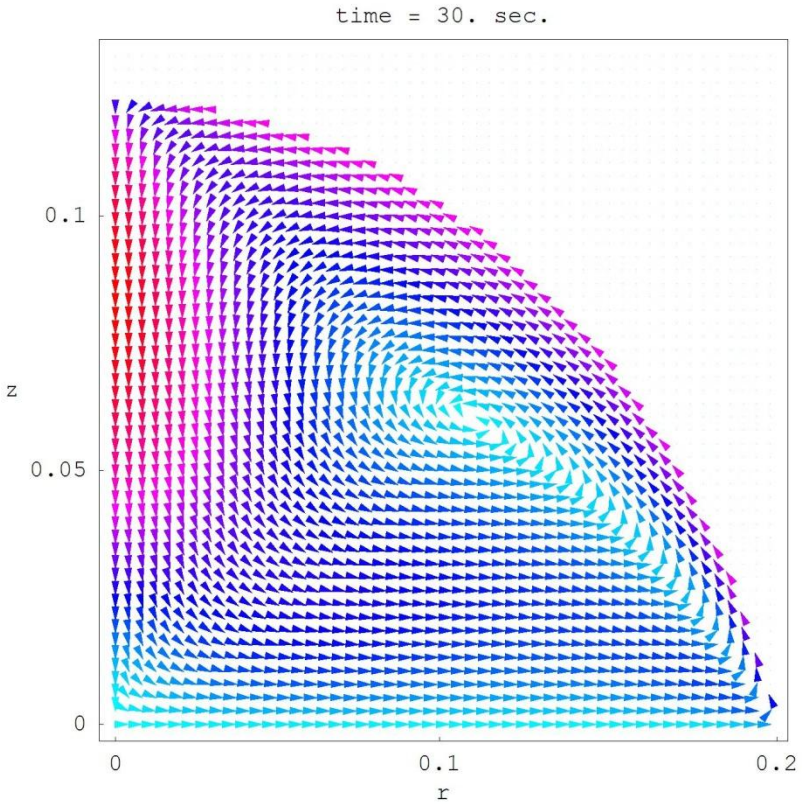

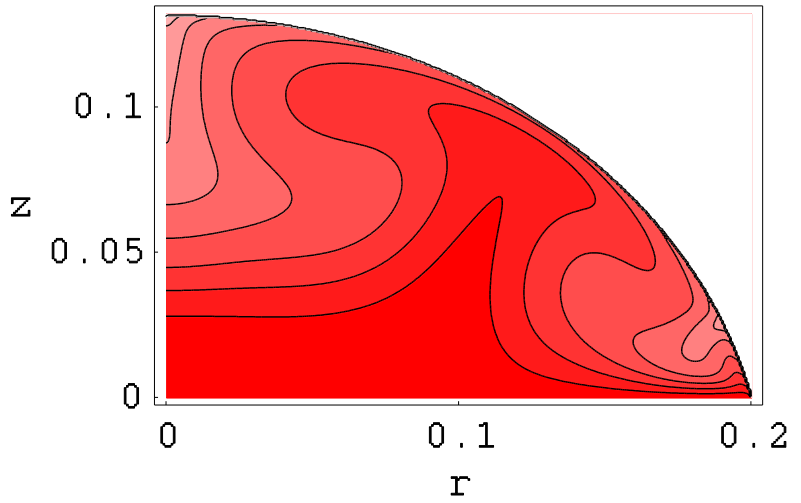

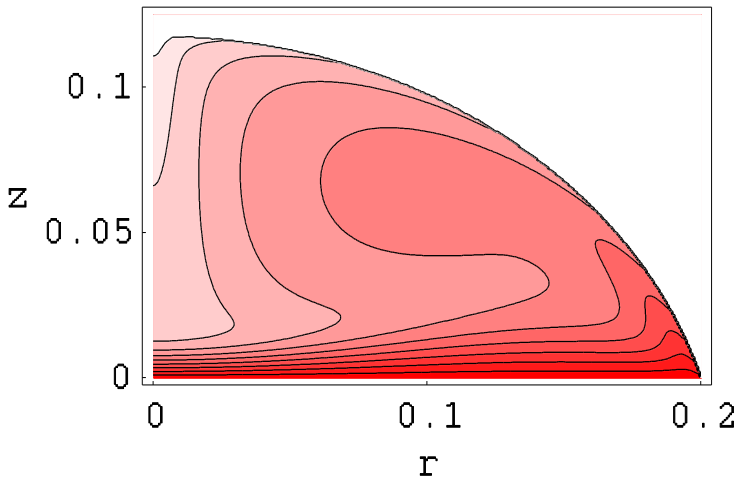

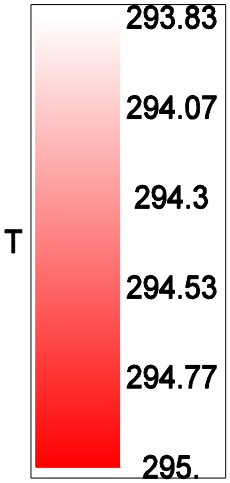

An overview of the numerical method

Fluid dynamics and thermal conduction

$$\frac{\partial \mathbf{u}}{\partial t} + (\mathbf{u}\nabla)\mathbf{u} + \frac{1}{\rho} \cdot \operatorname{grad} p = \nu \cdot \Delta \mathbf{u} \quad (1)$$

$$\operatorname{div} \mathbf{u} = 0 \quad (2)$$

$$\frac{\partial T}{\partial t} + \mathbf{u}\nabla T = \kappa \Delta T \quad (3)$$

Taking the curl of both sides of (1), one obtains

$$\frac{\partial}{\partial t}\gamma(r,z) + (\mathbf{u}\nabla)\gamma(r,z) = \nu\left(\Delta\gamma(r,z) - \frac{\gamma(r,z)}{r^2}\right),$$

where $\gamma(r,z) = \frac{\partial u_r}{\partial z} - \frac{\partial u_z}{\partial r}$;

We define stream function ψ such that

$$\frac{\partial \psi}{\partial z} = r u_r$$

$$\frac{\partial \psi}{\partial r} = -r u_z$$

Then velocites automatically satisfy the requirement $u_r/r + \partial u_r/\partial r + \partial u_z/\partial z = 0$

$$\Delta\psi = r\gamma - 2u_z. \qquad \tilde{\Delta}\psi = \frac{\partial^2\psi}{\partial r^2} - \frac{1}{r}\frac{\partial\psi}{\partial r} + \frac{\partial^2\psi}{\partial z^2} = r\left(\frac{\partial u_r}{\partial z} - \frac{\partial u_z}{\partial r}\right) = r\gamma.$$

1. Диффузия пара в пространстве вне капли

$$\frac{\partial u}{\partial t} = D\Delta u \qquad (1)$$

Граничные условия: на поверхности капли $u = u_s$, вдали от капли $u = 0$, на осях $r = 0$ и $z = 0$ имеем $\partial u/\partial r = 0$ и $\partial u/\partial z = 0$ соответственно.

Сеточный метод: Неявная схема, неравномерная решетка, изменяемый шаг по времени, интерполяция величин на границе капли.

5. Вычисление массы испарившегося за малый промежуток времени пара и обновление кривой поверхности капли

2. Вычисление ψ и скоростей $\mathbf{u}$ внутри капли

$$\tilde{\Delta}\psi = \frac{\partial^2\psi}{\partial r^2} - \frac{1}{r}\frac{\partial\psi}{\partial r} + \frac{\partial^2\psi}{\partial z^2} = r\gamma(r,z) \quad (1)$$

$$\partial\psi/\partial z = ru_r \quad (2)$$

$$\partial\psi/\partial r = -ru_z \quad (3)$$

Граничные условия: $\psi = 0$ на всех границах: на поверхности капли и на осях $r = 0$ и $z = 0$.

Сеточный метод: Неявная схема, равномерная решетка, граничная интерполяция на поверхности.

3. Вычисление γ внутри капли

$$\frac{\partial}{\partial t}\gamma + (\mathbf{u}\nabla)\gamma = \nu\left(\Delta\gamma - \frac{\gamma}{r^2}\right) \qquad (1)$$

Граничные условия: $\gamma = 0$ при $r = 0$; $\gamma = \partial u_r/\partial z$ при $z = 0$; $\gamma = \partial\sigma/(\eta\partial\tau) + 2u_\tau(\partial\phi)/(\partial\tau)$ на поверхности капли, где $\partial\sigma/\partial\tau = -\sigma'\partial T/\partial\tau$ – производная поверхностного натяжения вдоль поверхности капли; поверхностное натяжение σ на поверхности капли связано с температурой T по экспериментальной формуле $\sigma(T) = \sigma_0 - \sigma'(T - T_0)$; для толуола $\sigma_0 = \sigma(T_0) = 28.3049$ g/sec^2, $\sigma' = 0.11867$ g/sec^2.

Сеточный метод: Явная схема, равномерная решетка, граничная интерполяция на поверхности.

4. Вычисление T внутри капли

$$\frac{\partial T}{\partial t} + \mathbf{u}\nabla T = \kappa \Delta T \qquad (1)$$

Граничные условия: $\partial T/\partial r = 0$ при $r = 0$; $T = T_0$ при $z = 0$; $\partial T/\partial n = -Q_0(r)/k = -LJ(r)/k$ на поверхности капли, где $Q_0(r)$ – скорость потери тепла с единичной площадки поверхности капли, которая найдена при моделировании испарения, $\vec{n}$ – нормаль к поверхности капли.

Сеточный метод: Явная схема, равномерная решетка, граничная интерполяция на поверхности.

4. Calculation of the temperature T inside the droplet and the substrate.

$$\frac{\partial T}{\partial t} + \mathbf{u} \cdot \boldsymbol{\nabla} T = \kappa \Delta T$$

The boundary conditions take the form $\partial T/\partial r = 0$ for $r = 0$; $\partial T/\partial n = -Q_0(r)/k$ at the drop surface. Here $Q_0(r) = LJ_s(r)$ is the rate of heat loss per unit area of the upper free surface, $\mathbf{n}$ is a normal vector to the drop surface, J_s is the local evaporation rate.

At the substrate–fluid interface we have the matching condition $k_S \partial T_S/\partial z = k_L \partial T_L/\partial z$. At the substrate–gas interface we have $\partial T_S/\partial n = 0$, where $\mathbf{n}$ is a normal vector to the substrate surface, since the thermal conductivity of the air is negligibly small. At the bottom of the substrate we have the boundary condition $T_S = T_0$.

We have used implicit finite difference method and the following mesh in the drop and the substrate: $r_i = R\left(1 - (n-i)^2/n^2\right)$, $i = 0, \ldots, n$; $r_i = R\left(1 + (i-n)^2/n^2\right)$, $i = n+1, \ldots, 3n/2$; $z_j = hj^2/n^2$, $j = 0, \ldots, n$, where h is the droplet height and $n = 200$. Inside the substrate, we use the following mesh: $r_{Si} \equiv r_i$, $i = 0, \ldots, n$; $z_{Sj} = jh_S/n$, $j = 0, \ldots, n$, where h_S is the substrate thickness. Such irregular mesh allows to substantially increase the accuracy of the calculation in the vicinity of the contact line.

We use a boundary interpolation in a vicinity of the drop surface.

Beside axisymmetric thermogravitational and thermocapillary convection, a more complicated convective motion in the form of cellular convection or longitudinal hydrothermal waves (HTWs) can develop inside the droplet as a result of Marangoni instability due to non-uniform temperature distribution, as was first demonstrated in (Sefiane et.al. Appl.Phys.Lett. 93, 074103 (2008)) and confirmed in the numerous consequent studies.

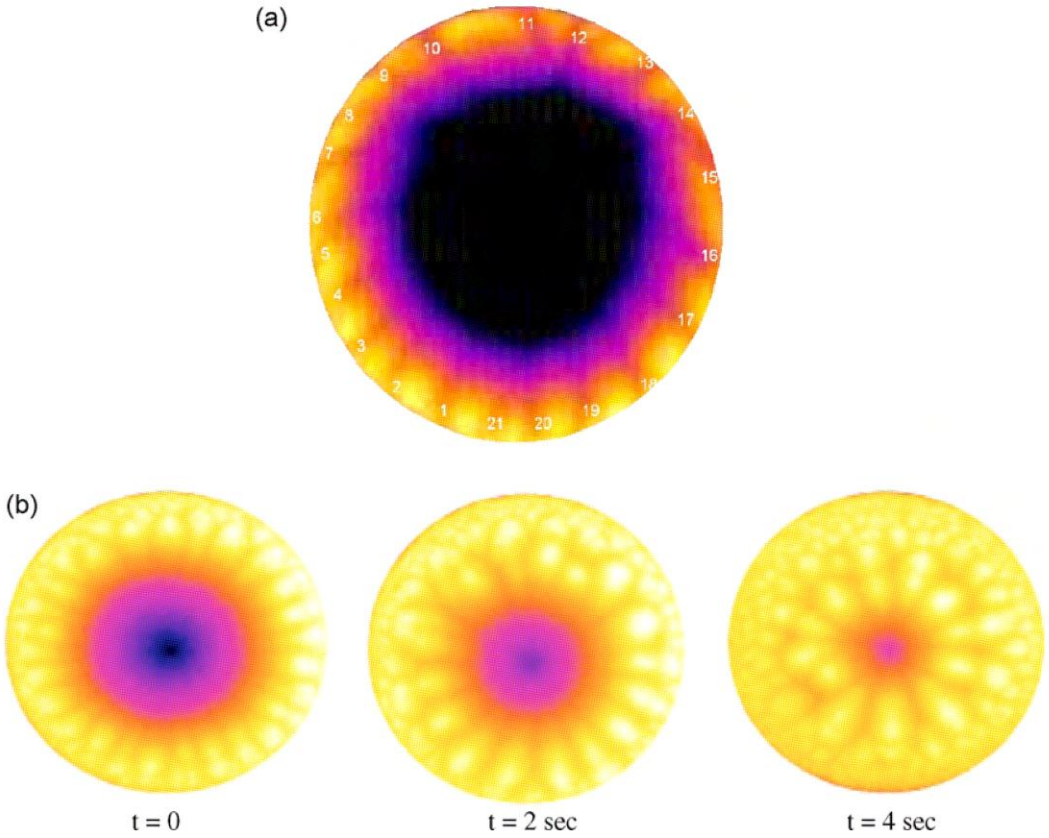

Fig. 4. (a) Evaporating methanol drops, thermal waves numbered across the drop circumference. (b) Evolution of the patterns observed during the evaporation of a FC-72 drop on a titanium substrate.

Experimental study: infrared thermography.
The process of evaporation is composed of three phases:

Phase 1 Warming up of the drop – The start of the experiment is defined as the initial contact of the drop on the substrate which is characterized by a sharp increase of the heat flux. The first seconds of the experiments are characterized by a transitional phenomenon. The drop, which was initially at room temperature, is placed on a warm surface and is first heated to reach almost the substrate temperature. The first step of the phenomenon is thus only driven by the heat capacity of the fluid.

Phase 2 Drop evaporation – The heat flux reaches a maximum value which corresponds to the beginning of our evaporation investigation. During this principal phase of evaporation, we can observe the appearance and the evolution of thermal-convective instabilities. The heat flux during over phase decrease continuously. Depending on the fluid, different kinds of these instabilities seem to be observed.

Phase 3 Film evaporation – A second phase of evaporation is characterized by the decrease of the heat flux when the convection cells have disappeared. The shape of the drop looks more like a layer than a drop. The evaporation rate is thus closer to film evaporation than drop evaporation.

- Instability type and characteristics depend essentially on the volatility of liquid used, which to a large extent governs the temperature gradients arising
- no instability has been detected by evaporation of water droplet;
- HTWs moving in azimuthal direction have been observed for more volatile methanol and ethanol;
- and convective cells emerging near the droplet apex and drifting to the edge developed when even more volatile Fluorinert FC-72 has been used.
- The number of waves in a more volatile liquid (methanol) has been larger in comparison to ethanol.
- The number of waves observed increased with the increase of thermal conductivity and substrate temperature. The number of waves depends also on the droplet age, i.e. on its height. The smaller is the droplet height the smaller is the number of waves.
- For cellular convection (FC-72) the cells are larger near the droplet apex, where the temperature is lower. There is a region of small cells near the three-phase contact line. With time, as the droplet evaporates, the temperature gradient across the surface becomes smaller and the region occupied by small cells broadens

The theoretical treatment of the convective instabilities accompanying the droplet evaporation is complicated because

- the problem is essentially 3-dimensional;
- the profile of the droplet changes with time;
- there is coupling between the heat transfer in three phases (solid substrate, liquid and vapour) and mass transfer in two fluid phases (liquid and vapour);
- evaporation rate depends on the solid/liquid contact angle.

Dimensionless numbers and scaling in the HTW probem:
[K. Sefiane et. al., Colloids Surf. A 365, 95 (2010)].

The Lubrication Approximation

The lubrication approximation for an evaporating droplet of capillary size was derived by Hu and Larson in 2005. The derivation includes three basic assumptions which are justified for $\theta \ll 1$:

a) The radial velocity $u_r(z)$ at each value of r has a quadratic dependence on z.

b) The droplet free surface is approximated as a parabola $h(\tilde{r}, t) = h(0, t)(1 - \tilde{r}^2)$, where $\tilde{r} = r/R$.

c) The total shear stress at the droplet free surface is approximated by the rz-component of the stress tensor.

Heuristic extension of the lubrication approximation

The following equations are applicabel for arbitrary $T(r)$ and $h(r)$, reduce to the lubrication solution obtained by Hu and Larson for small contact angles, where $h(\tilde{r},t) = h(0,t)(1-\tilde{r}^2)$, and they precisely satisfy the continuity equation for arbitrary contact angle.

$$\tilde{u}_r = \frac{3}{8}\frac{1}{1-\tilde{t}}\frac{1}{\tilde{r}}\left[(1-\tilde{r}^2)-(1-\tilde{r}^2)^{-\lambda}\right]\left(\frac{\tilde{z}^2}{\tilde{h}^2}-2\frac{\tilde{z}}{\tilde{h}}\right)+$$

$$+\frac{\tilde{r}h_0^2\tilde{h}}{R^2}\left(\tilde{J}\lambda(1-\tilde{r}^2)^{-\lambda-1}+1\right)\left(\frac{\tilde{z}}{\tilde{h}}-\frac{3}{2}\frac{\tilde{z}^2}{\tilde{h}^2}\right)+\frac{M_a h_0\tilde{h}}{2R}\frac{d\tilde{T}}{d\tilde{r}}\left(\frac{\tilde{z}}{\tilde{h}}-\frac{3}{2}\frac{\tilde{z}^2}{\tilde{h}^2}\right), \quad (3)$$

$$\tilde{u}_z = \frac{3}{4}\frac{1}{1-\tilde{t}}\left(1+\lambda(1-\tilde{r}^2)^{-1-\lambda}\right)\left(\frac{\tilde{z}^3}{3\tilde{h}^2}-\frac{\tilde{z}^2}{\tilde{h}}\right)-\frac{3}{4}\frac{\left[(1-\tilde{r}^2)-(1-\tilde{r}^2)^{-\lambda}\right]}{1-\tilde{t}}\times$$

$$\times\left(\frac{\tilde{z}^2}{2\tilde{h}^2}-\frac{\tilde{z}^3}{3\tilde{h}^3}\right)\frac{1}{\tilde{r}}\frac{\partial\tilde{h}}{\partial\tilde{r}}-\frac{h_0^2}{R^2}\left(\tilde{J}\lambda(1-\tilde{r}^2)^{-\lambda-1}+1\right)\left(\tilde{z}^2-\frac{\tilde{z}^3}{\tilde{h}}\right)-$$

$$-\frac{\tilde{r}^2h_0^2}{R^2}\tilde{J}\lambda(\lambda+1)(1-\tilde{r}^2)^{-2-\lambda}\left(\tilde{z}^2-\frac{\tilde{z}^3}{\tilde{h}}\right)-\frac{\tilde{r}h_0^2}{R^2}\left(\tilde{J}\lambda(1-\tilde{r}^2)^{-\lambda-1}+1\right)\frac{\tilde{z}^3}{2\tilde{h}^2}\frac{\partial\tilde{h}}{\partial\tilde{r}}-$$

$$-\frac{M_a h_0}{4R}\left(\frac{d^2\tilde{T}}{d\tilde{r}^2}+\frac{1}{\tilde{r}}\frac{d\tilde{T}}{d\tilde{r}}\right)\left(\tilde{z}^2-\frac{\tilde{z}^3}{\tilde{h}}\right)-\frac{M_a h_0}{4R}\frac{d\tilde{T}}{d\tilde{r}}\frac{\tilde{z}^3}{\tilde{h}^2}\frac{\partial\tilde{h}}{\partial\tilde{r}}. \quad (4)$$

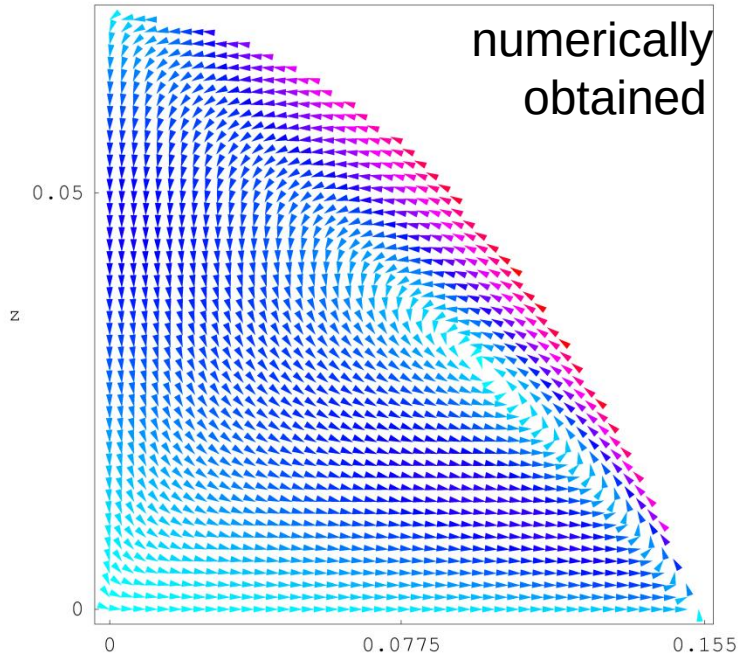
numerically obtained
0.05
z
0
0
0.0775
0.155

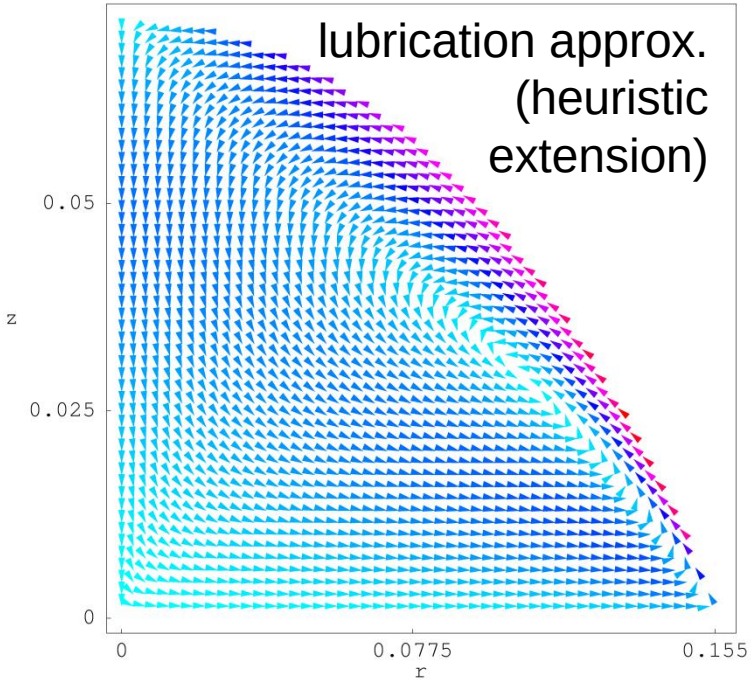
lubrication approx. (heuristic extension)
0.05
z
0.025
0
0
0.0775
0.155
r

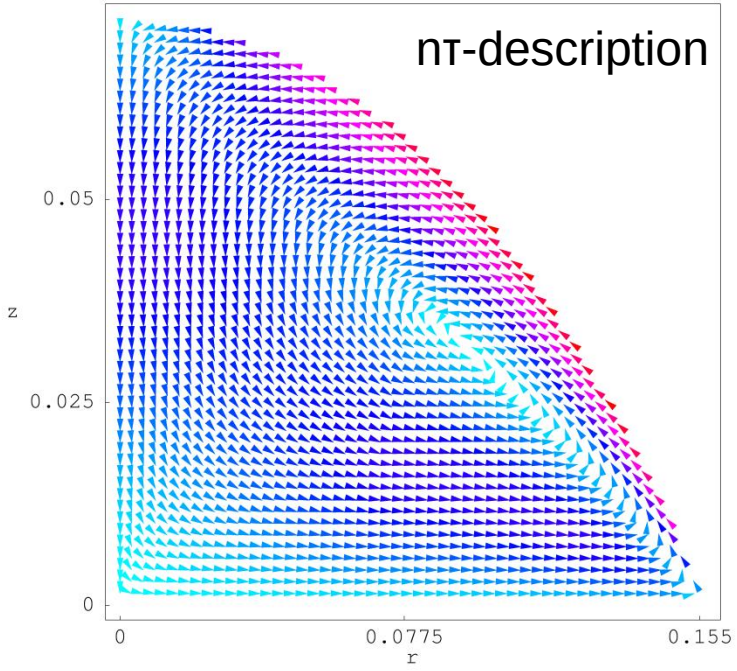
nτ-description
0.05
z
0.025
0
0
0.0775
0.155
r

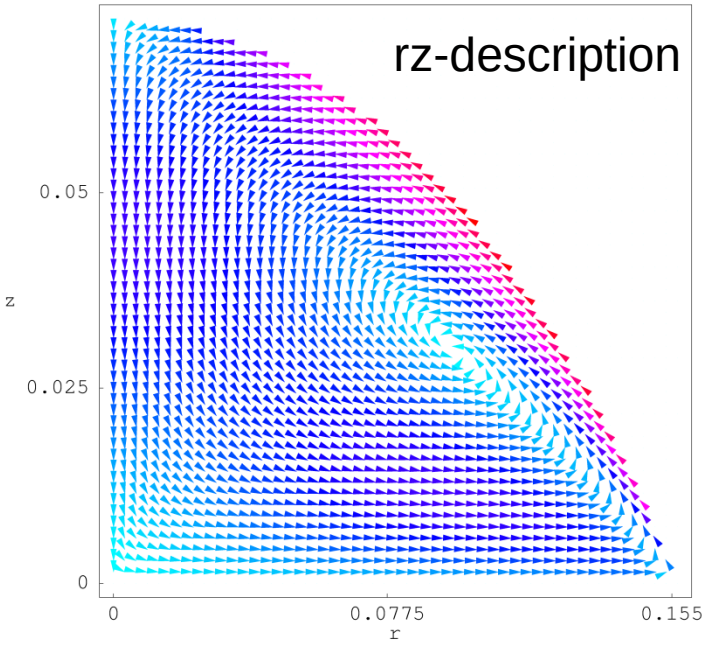
rz-description
0.05
z
0.025
0
0
0.0775
0.155
r

The surface velocity for the toluene droplet. Left panel: $\theta = 50°$, right panel: $\theta = 20°$. Blue curve is the numerically obtained surface velocity. Green curve: the surface velocity in the heuristic extension of the lubrication approximation. Purple curve: the surface velocity in the $n\tau$-description. Red curve: the surface velocity in the rz-description. Here the Marangoni number exceeds 3000, and the numerical results contain the "bottleneck" effect.

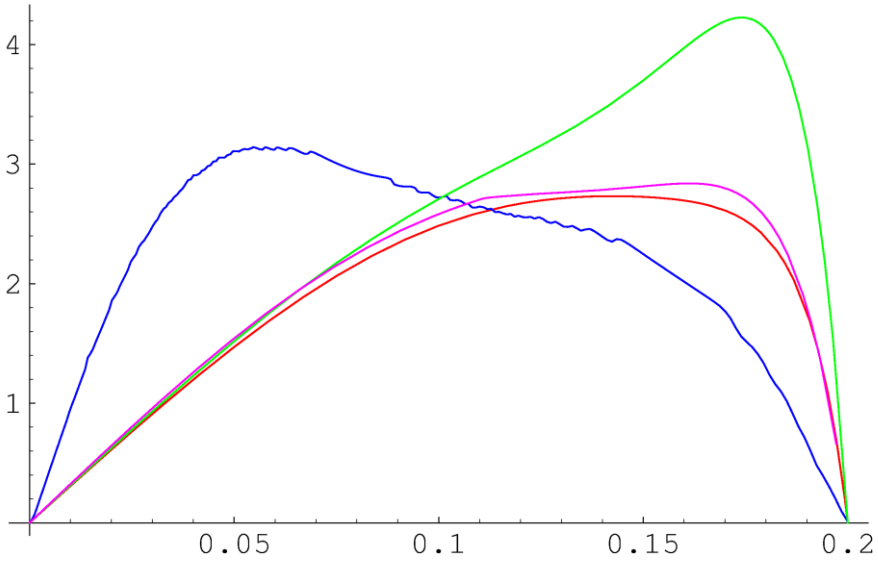

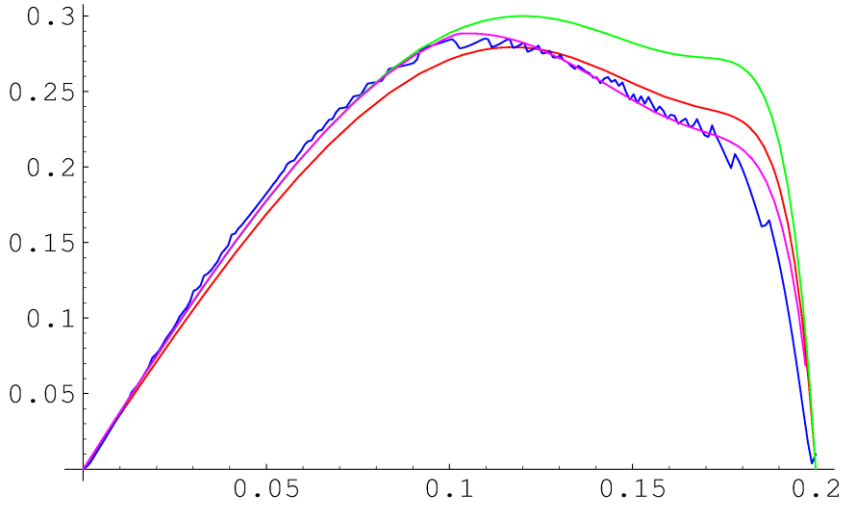

Ristenpart et.al., Phys. Rev. Lett.99, 234502 (2007)

$$\nabla^2 T = 0,$$

$$j(x) = j_0[1 - (x/R)^2]^{-1/2+\theta_c/\pi},$$

$$-k_L \mathbf{n} \cdot \nabla T = \Delta H_v j(x) \quad \text{at} \quad y = h(x),$$

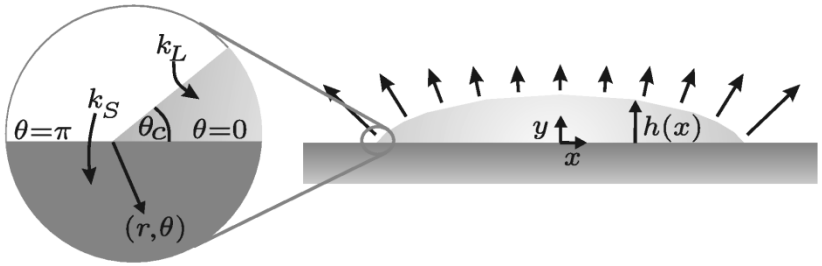

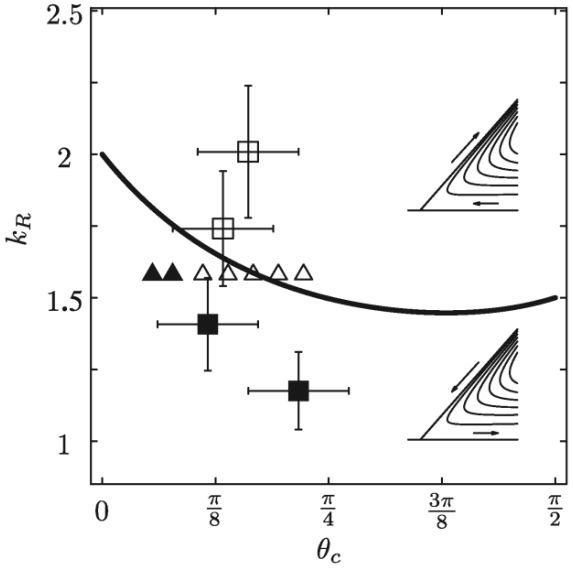

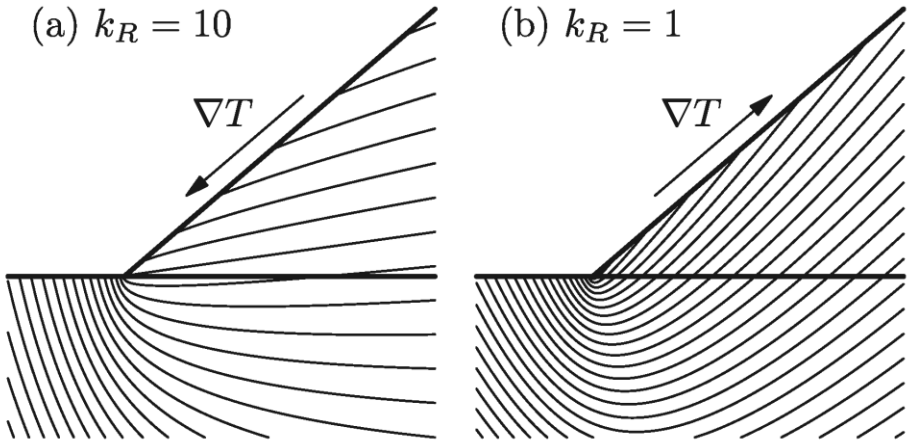

Xu et.al., Langmuir 26(3), 1918-1922 (2010)

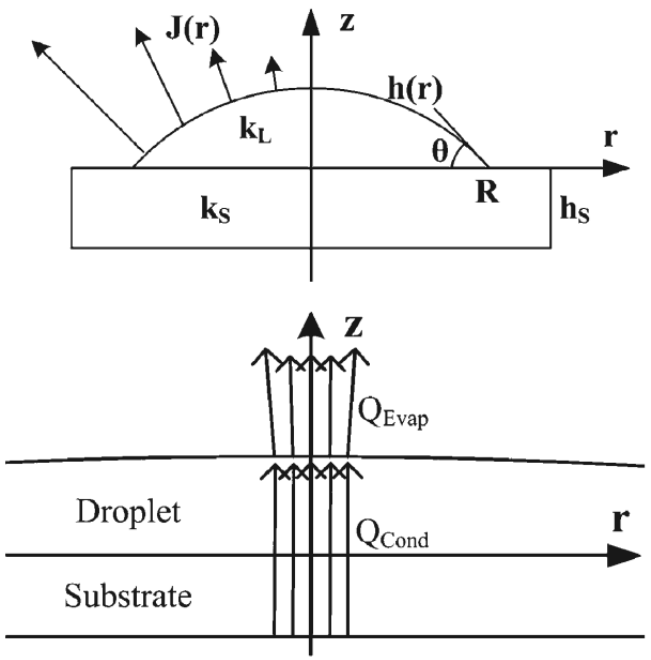

$$R_N \equiv h_R/k_R \equiv h_S k_L/Rk_S.$$

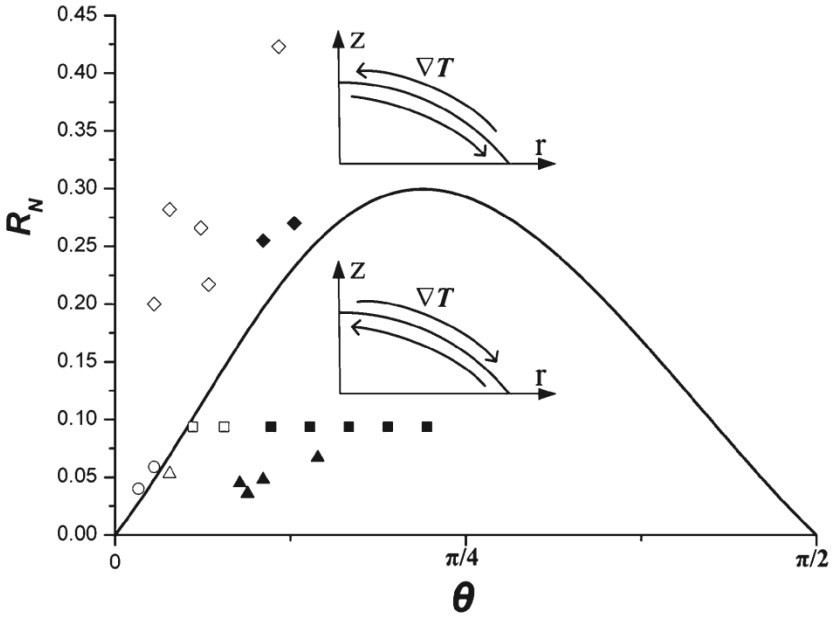

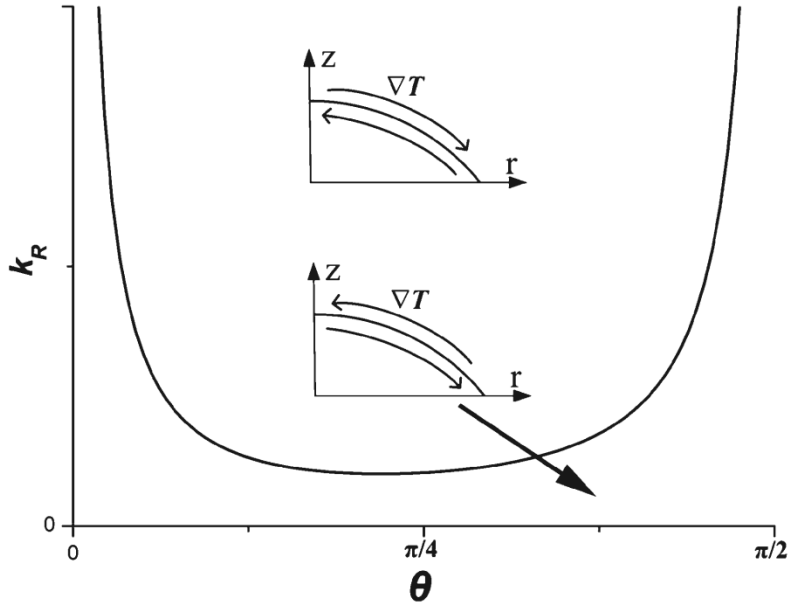

Results of Zhang et.al., Phys. Rev. E **89**, 032404 (2014)

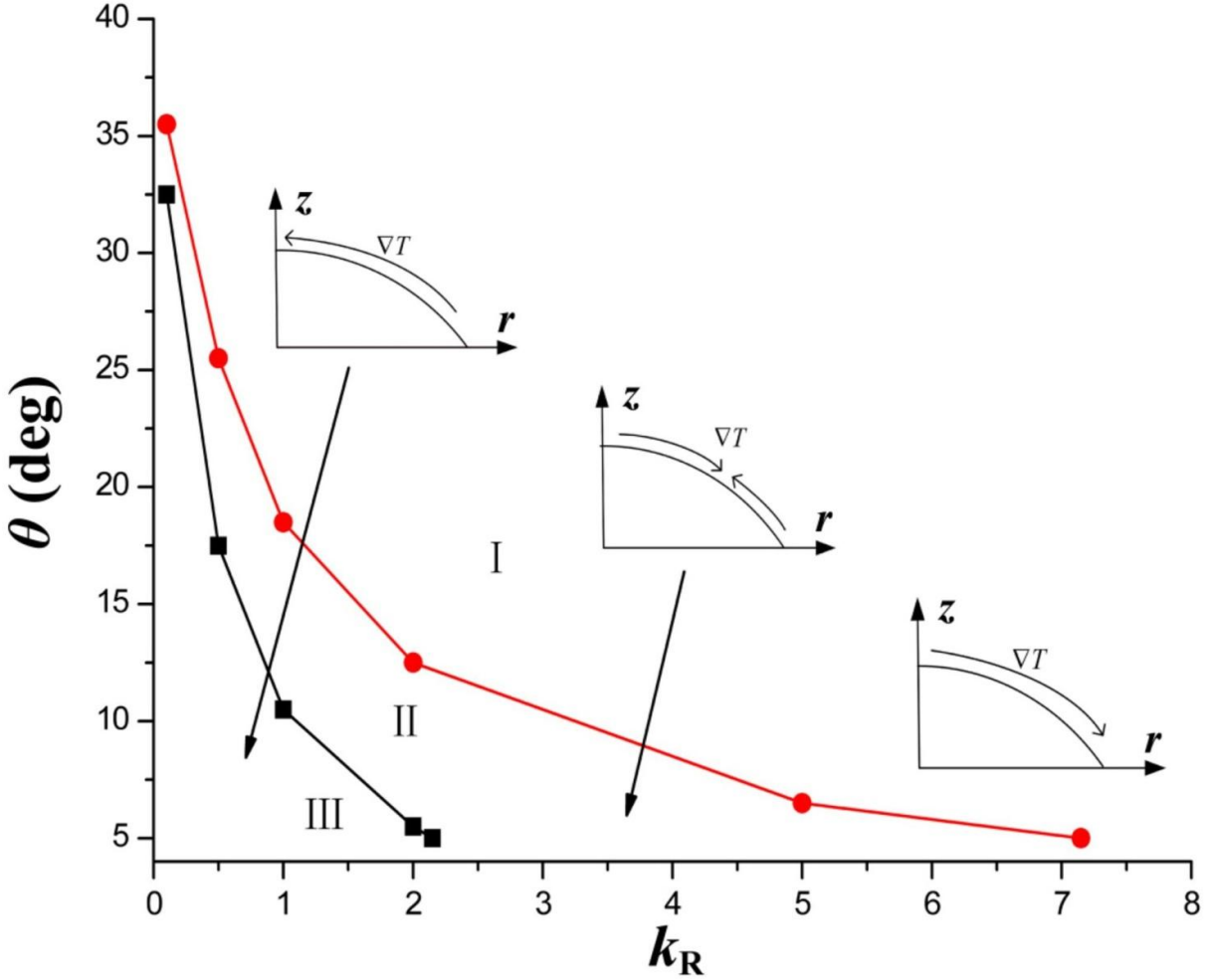

FIG. 5. (Color online) "Phase diagram" for the temperature distribution along the surface of drying droplet on substrates with the relative thickness of $h_R = 0.1$. The data points were obtained from numerical simulations.

FIG. 1: Temperature distribution, distribution of absolute value of velocity and vector field plot of velocity for a droplet of 1-hexanol in a single-vortex regime obtained for $\theta = 35^\circ$, $k_R = 1$, $h_R = h_S/R = 0.05$.

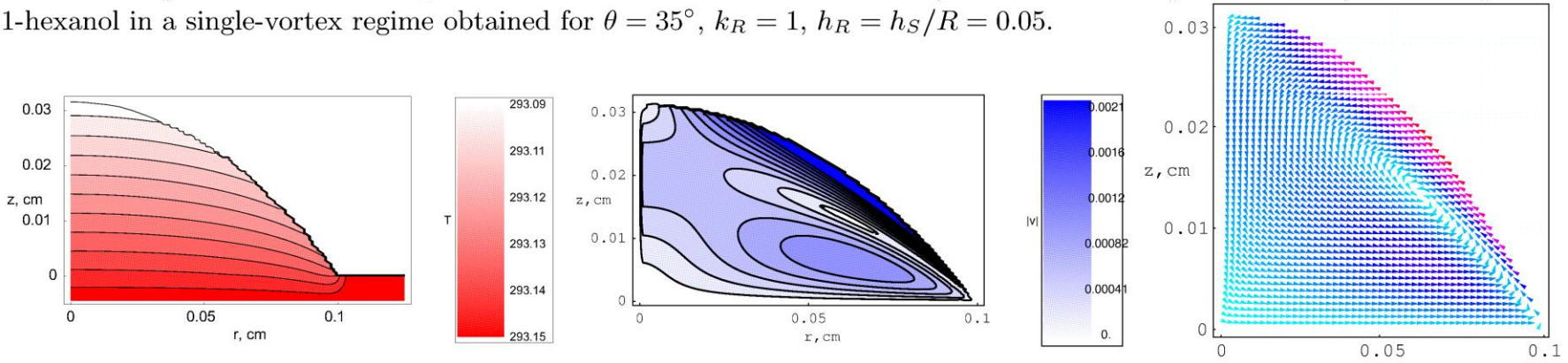

FIG. 2: Temperature distribution inside the droplet and the substrate correspondingly, distribution of absolute value of velocity and vector field plot of velocity in a reversed single-vortex regime obtained for 1-hexanol, $\theta = 35^\circ$, $k_R = 0.01$, $h_R = h_S/R = 0.05$.

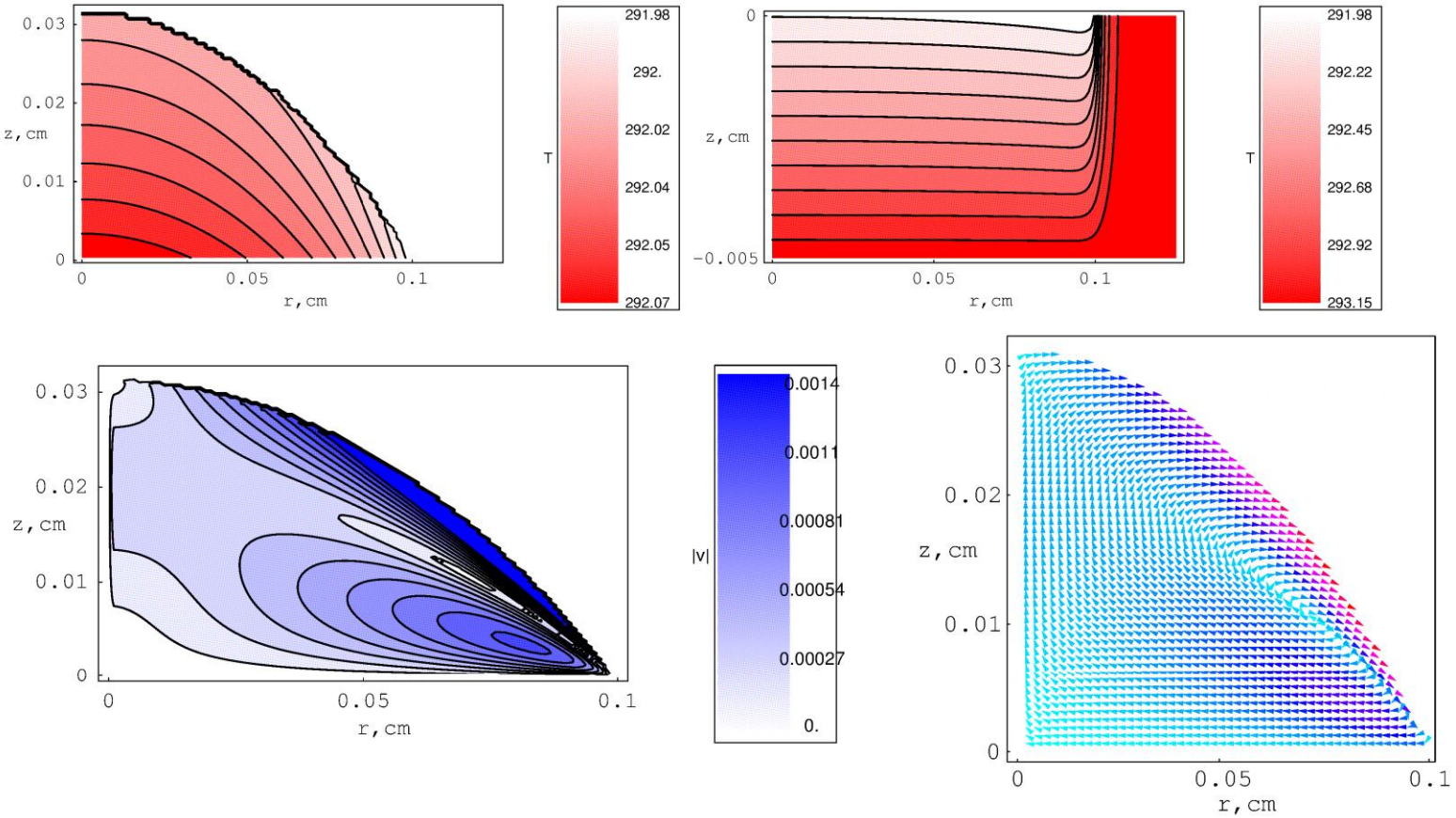

FIG. 3: Temperature distribution inside the droplet and the substrate correspondingly, distribution of absolute value of velocity and vector field plot of velocity for a droplet of 1-hexanol in a two-vortex regime obtained for $\theta = 22.44^\circ$, $k_R = 0.2$, $h_R = h_S/R = 0.5$.

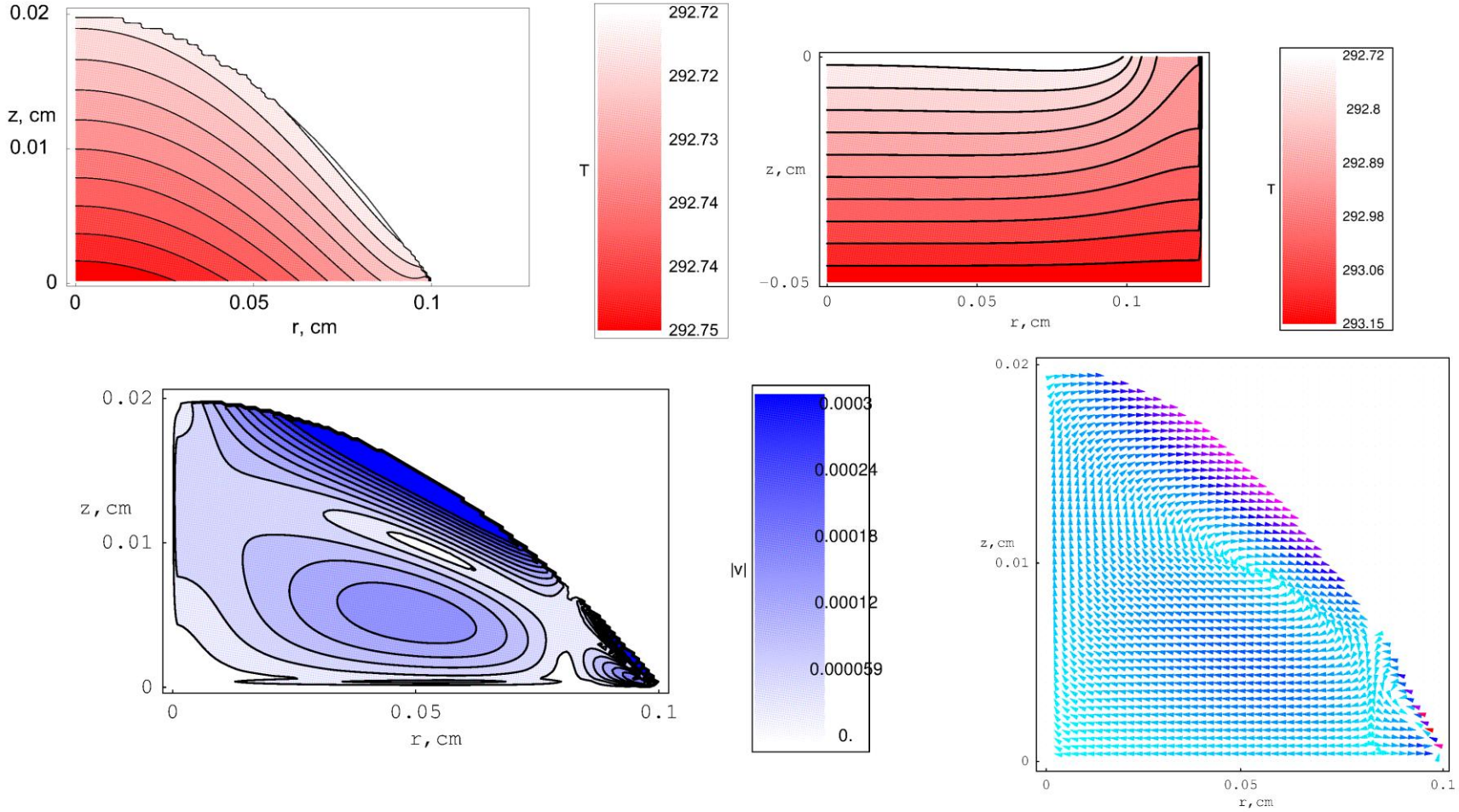

FIG. 4: Temperature distribution inside the droplet and the substrate correspondingly, distribution of absolute value of velocity and vector field plot of velocity for a droplet of 1-hexanol in a three-vortex regime obtained for $\theta = 31.22°$, $k_R = 0.2$, $h_R = h_S/R = 0.1$.

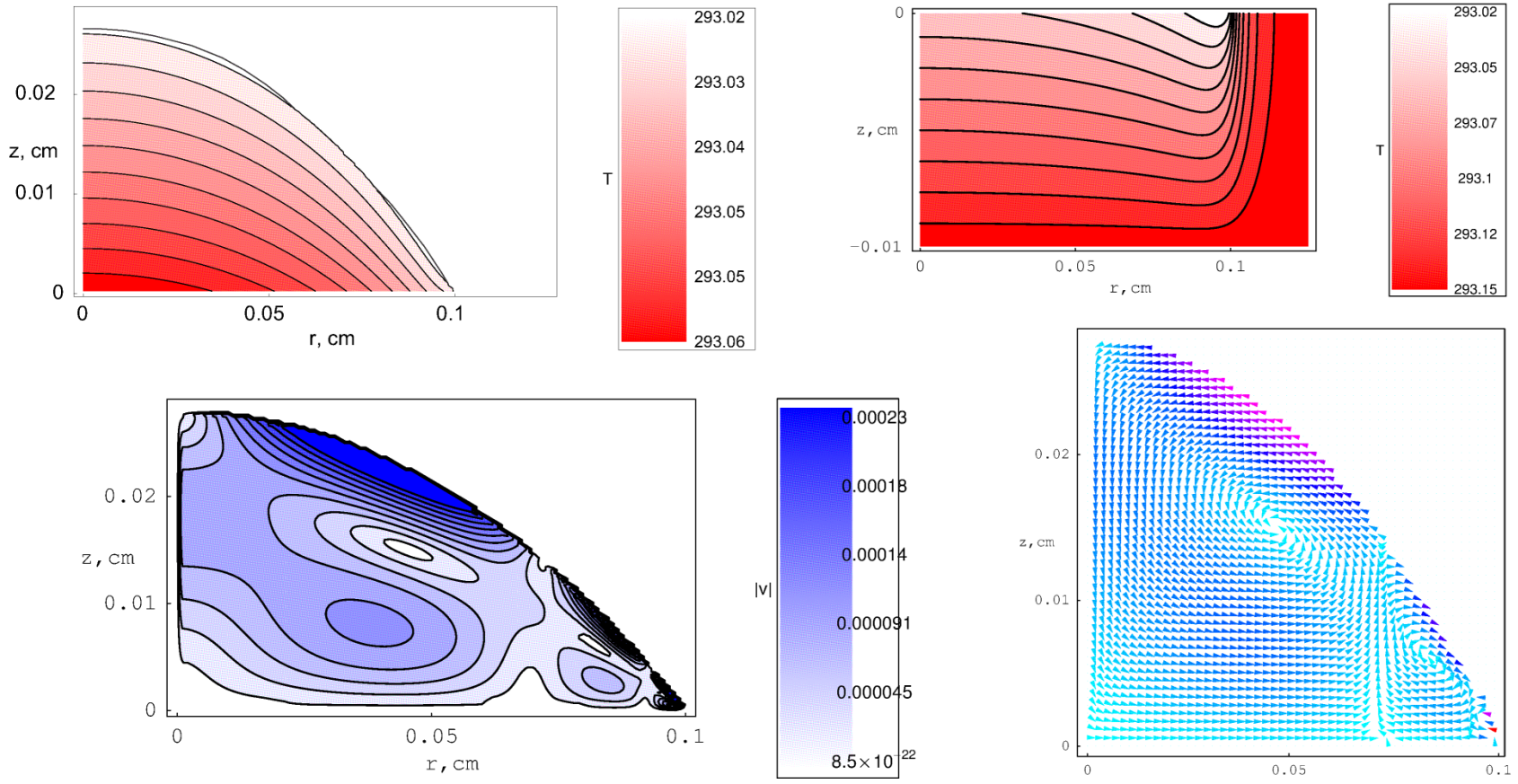

FIG. 5: Surface temperature distribution for a single-vortex, reversed single-vortex, two-vortex and three-vortex regimes corresponding to the 1-hexanol droplets in Figs. 1-4.

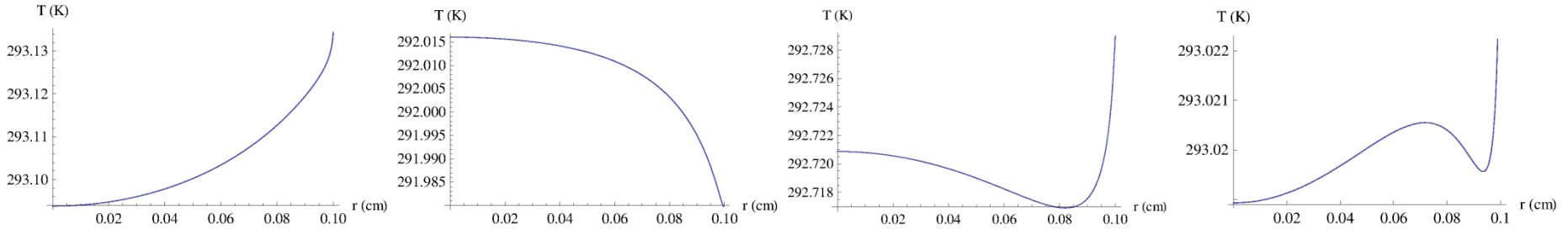

FIG. 6: Results for θ vs $k_R = k_S/k_L$, where a) $h_R = 0.01$, b) $h_R = 0.05$, c) $h_R = 0.1$, d) $h_R = 0.2$, e) $h_R = 0.5$, f) $h_R = 1$.

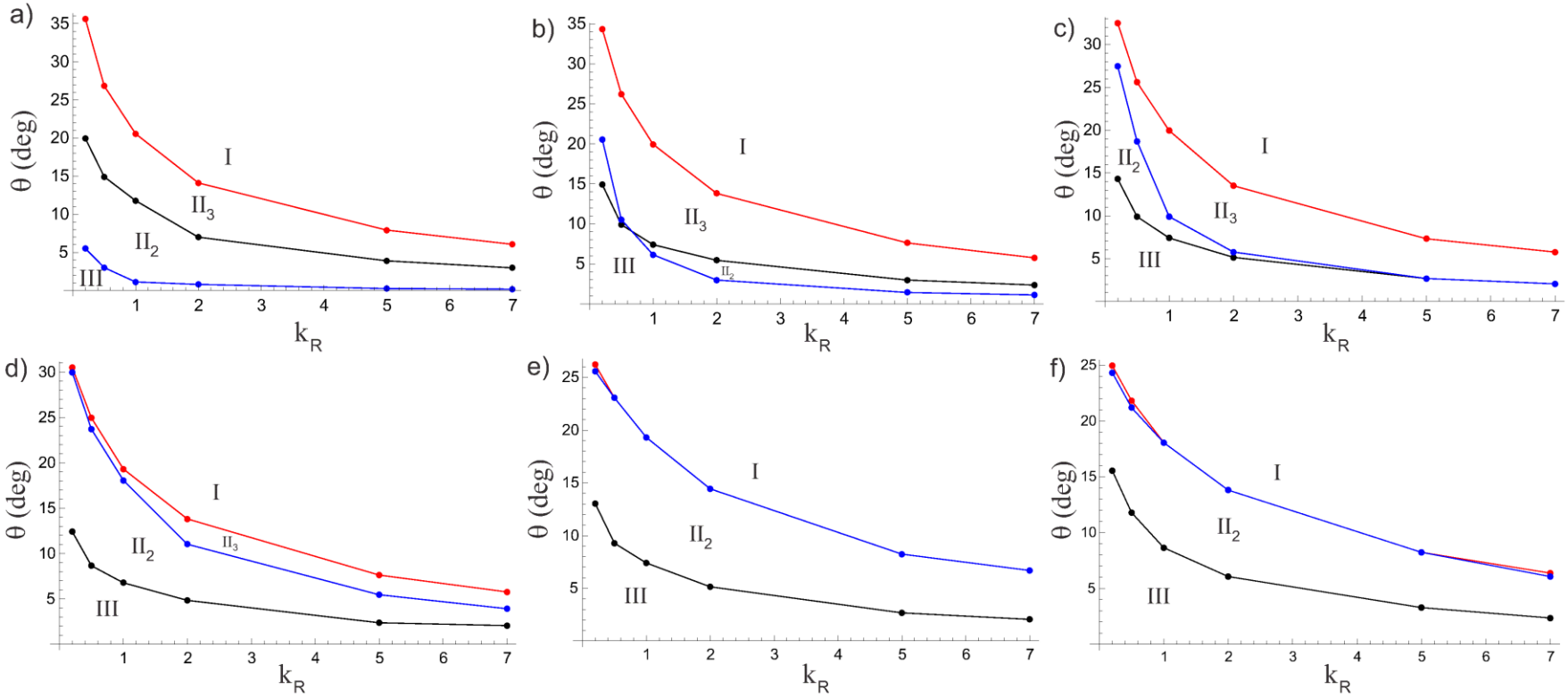

FIG. 7: Dependence of θ_{crit} on $h_R = h_S/R$ for a) the transition corresponding to the change of sign of tangential component of the temperature gradient at the liquid-vapor interface near the contact line; b) the transition to a monotonically increasing surface temperature dependence on r; c) the transition corresponding to the change of sign of tangential component of the temperature gradient at the liquid-vapor interface near the droplet apex.

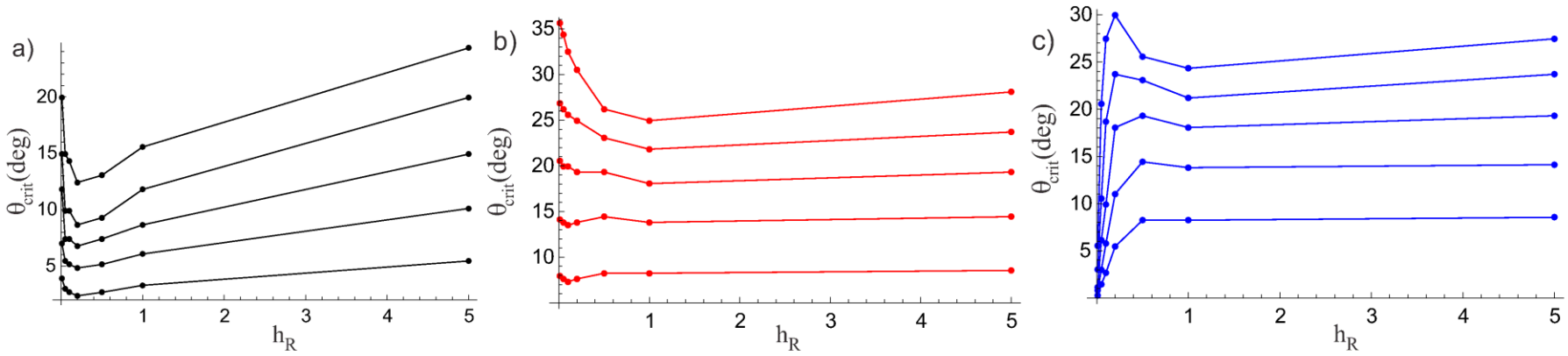

Results for θ (deg) vs k_R, where $h_R = 0.1$.

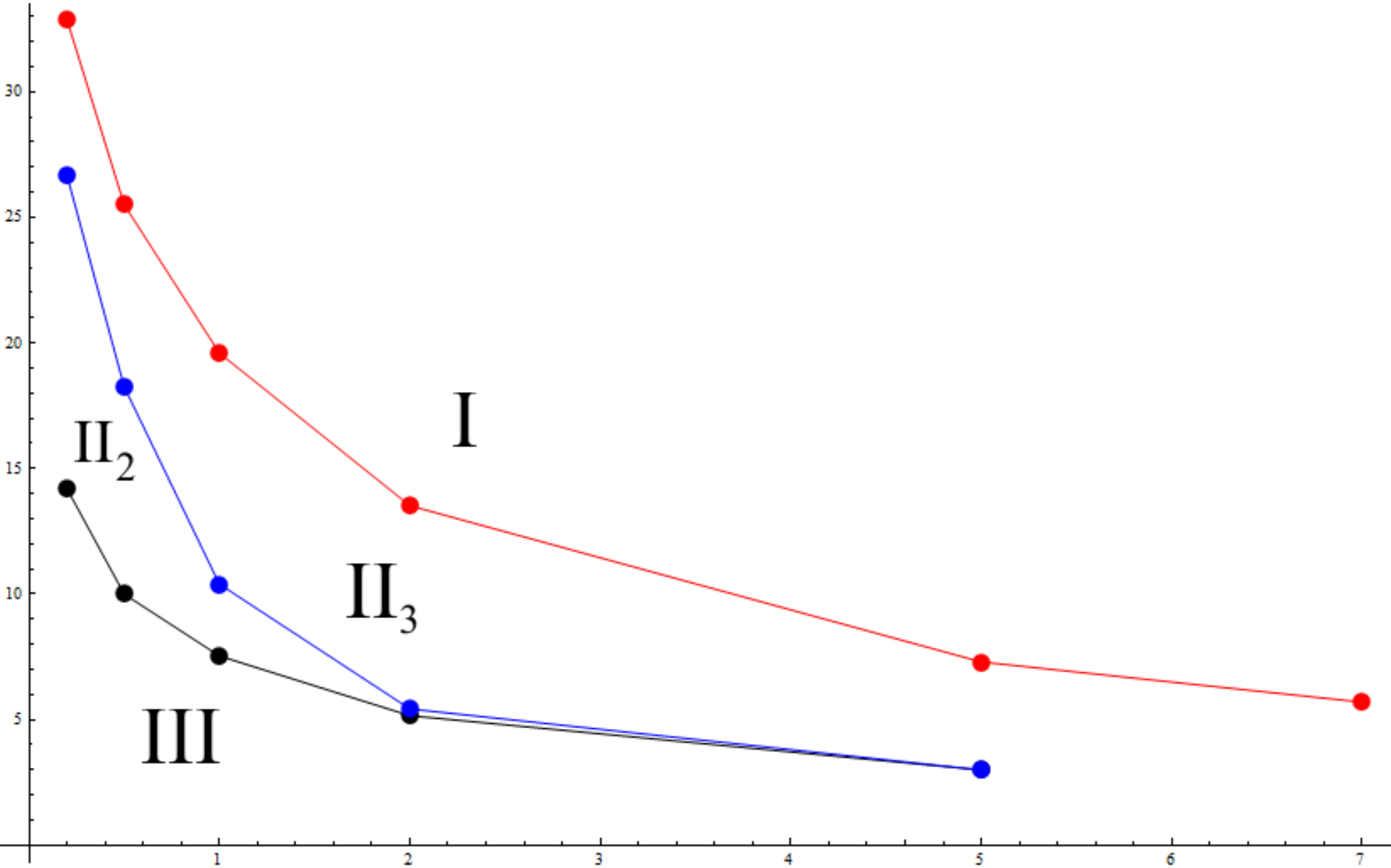

Results for θ (deg) vs k_R, where $h_R = 0.2$.

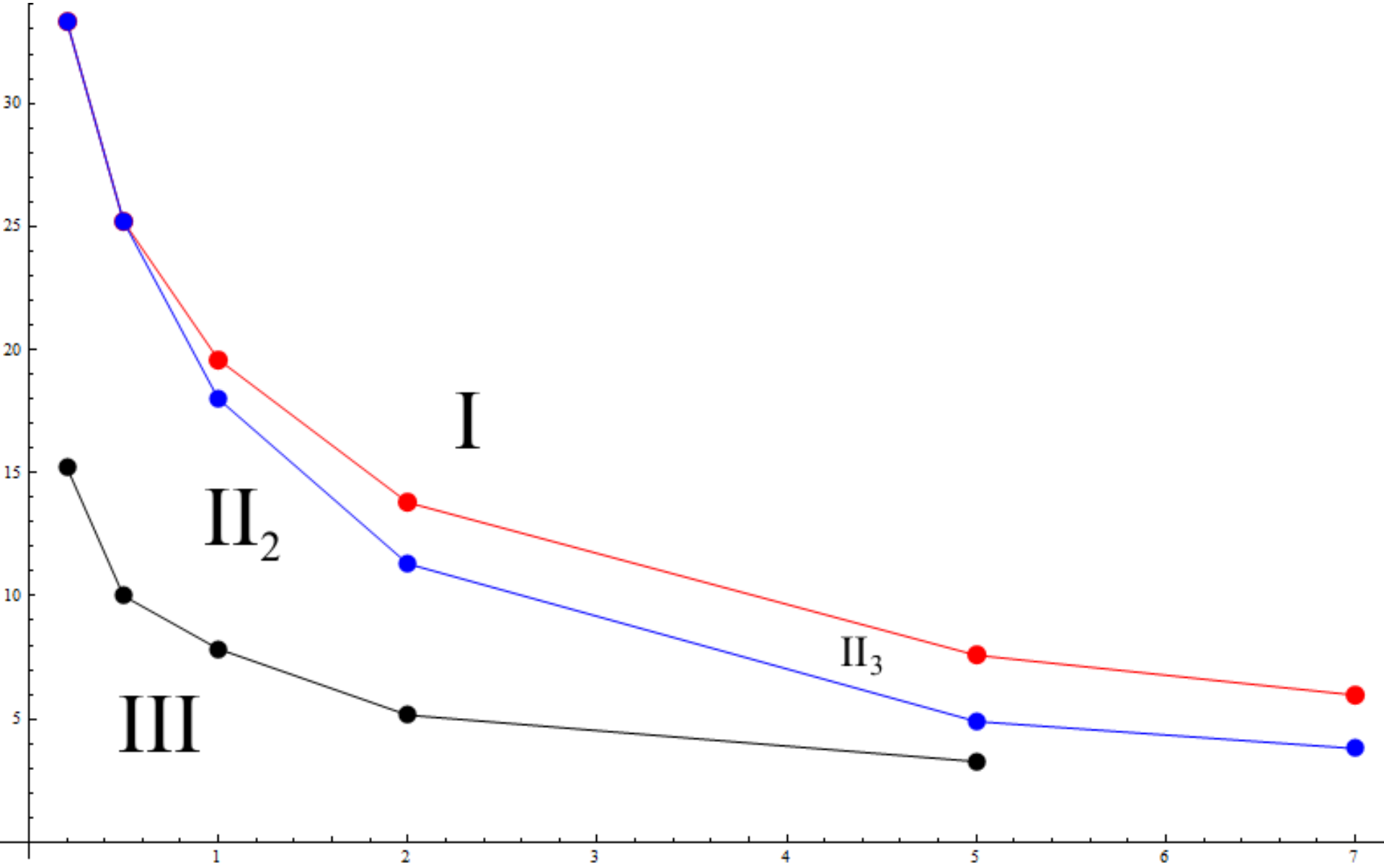

Results for θ (deg) vs k_R, where $h_R = 0.8$.

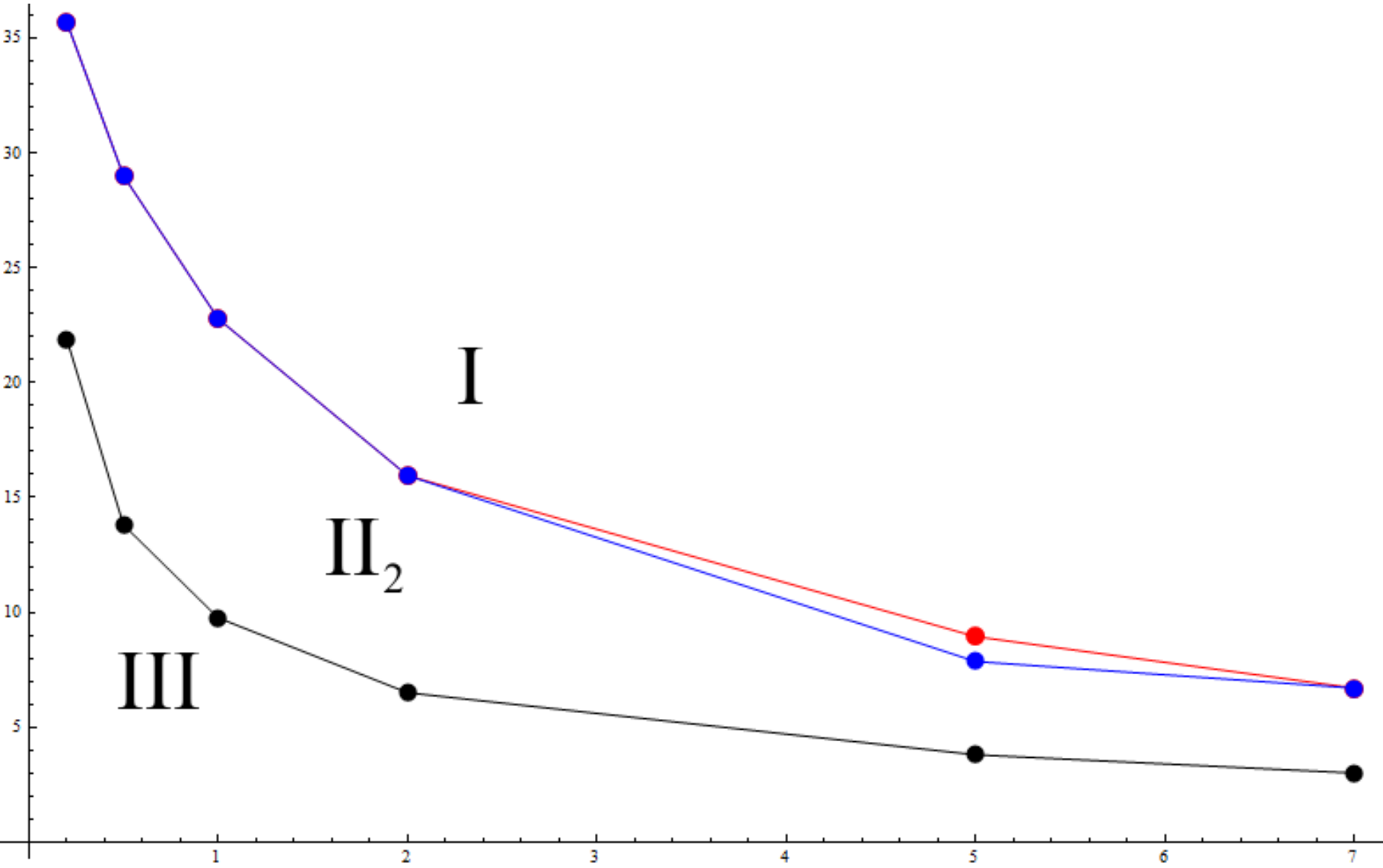

Results for θ (deg) vs k_R, where $h_R = 6.4$.

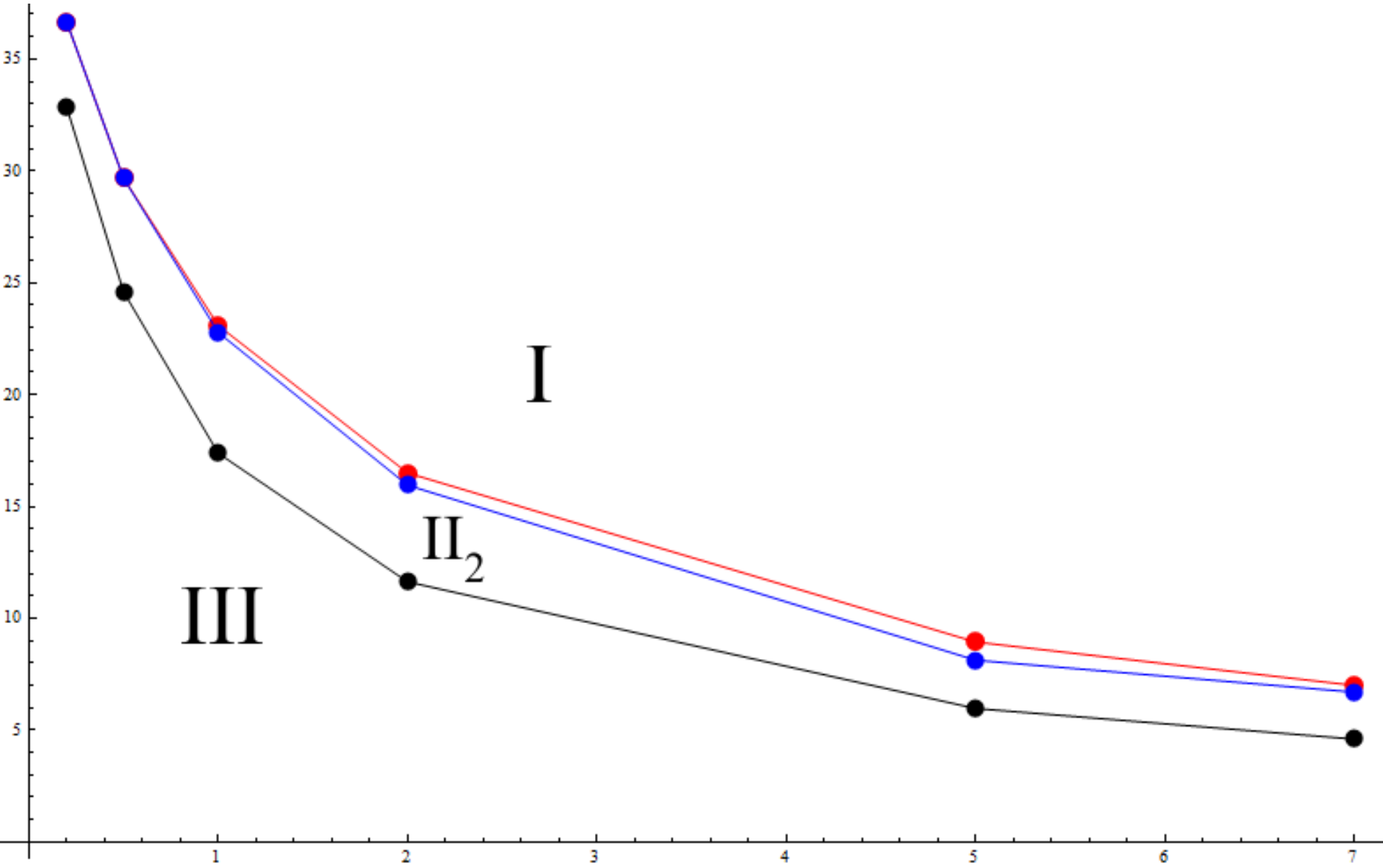

Part II - Conclusions

- The fluid flow structure in an evaporating sessile droplet of capillary size has been considered in disregarding the convective heat transfer, i.e., for relatively small and slowly evaporating droplets (when $Pe = \overline{u}R/\kappa \ll 1$). It is shown that the region II of the "phase diagram" consists of the two subregions II_2 and II_3, where II_2 corresponds to the flows with two vortices and II_3 corresponds to the flows with three vortices. The transition between the regions III and II_2 corresponds to the change of sign of the tangential component of the temperature gradient at the liquid-vapor interface either at the droplet apex (for small substrate thickness) or near the contact line (for larger substrate thickness). The transition between the regions II_2 and II_3 corresponds to the change of sign of the tangential component of the temperature gradient at the liquid-vapor interface either near the contact line (for small substrate thickness) or at the droplet apex (for larger substrate thickness). Further increase of the substrate thickness makes subregion II_2 dominating in region II, and results in a shift of the regions I and II to larger contact angles.

- Temperature distribution, fluid flow structure in the droplet and general form of a "phase diagram" can be qualitatively understood as a result of matching the heat transfer through the solid-liquid interface and the vaporization heat, which flows through the liquid-vapor interface.

- The results obtained demonstrate that the fluid flow structure in evaporating droplets of capillary size can be prepared in a controlled manner by selecting substrates with appropriate thermal conductivity and thickness.